

The Comparison of RDG-FA and T-matrix Models by Considering Primary Particles Polydispersity and Effective Density of Soot Aggregates

Keyhan Babaee*, Timothy A Sipkens*, Steven N Rogak†

Department of Mechanical Engineering, University of British Columbia, Vancouver, Canada
2329 West Mall, BC, V6T 1Z4, Canada

Abstract

This work presents an approach to calculate and compare the optical properties of soot aggregates using Rayleigh-Debye-Gans approximation for soot fractal-like aggregates (RDG-FA) and the multiple-sphere T-matrix method by considering the fact that primary particle size and effective density of the aggregates change with aggregate mobility diameter for non-premixed flames. The distribution of primary particle size was characterized by the geometric standard deviation of primary particle size for a specified aggregate mobility diameter. Primary particle size is assumed constant within each aggregate. For RDG-FA, we use the developed model by Babaee et al. (2019). This study implements and reconfigures T-matrix database developed by Liu et al. (2019) to calculate total absorption and scattering cross-section of soot aggregates. Soot fractal aggregates with the refractive index of $1.6+0.6j$ at 532 nm, $1.95+0.79j$ at 550 nm, and $2+j$ at a wavelength of 870 nm were selected as a case study, and a parametric study is undertaken to determine the sensitivity of the optical properties of the aggregate to the mass-mobility exponent, effective density, and primary particle size distribution.

1. Introduction

Soot plays a critical role in climate and weather changes [1]. However, the extent of its impact is poorly understood as there are large uncertainties associated with how soot interacts with light in the atmosphere. This is complicated by the fact that soot often forms fractal-like aggregates, such that the radiative properties will depend on both the composition and morphology of the particles [2].

Several methods are available to estimate the optical properties of soot, including the T-matrix [3] and discrete dipole approximation (DDA) [4] approaches. However, these more advanced methods require detailed information of the shape of the soot aggregates and are computationally intensive. This means that they are not practical for climate modeling, and researchers often instead employ Rayleigh-Debye-Gans theory for fractal-like aggregates (RDG-FA). Derived from Lorenz-Mie theory [5], RDG-FA neglects spherule-to-spherule interactions such that the absorption cross section of an individual aggregate is equal to the sum of the absorption cross section of primary particles within the aggregate. This allows for a simple route to evaluate the mass-scattering coefficient (MSC) as a summary parameter to characterize how the particles scatter light [6].

This work seeks to integrate the calculation of the MAC and MSC predicted by RDG-FA with the existing relations governing aggregate mobility diameter, primary particle diameter, and mass. Specifically, recent work [7] on soot generated from non-premixed flames has suggested that (i) the primary particle diameter is roughly constant within aggregates and (ii) that the mean primary particle diameter within an aggregate scales with its mobility diameter (cf. Fig. 1). To this end, Section 2 discusses the relations governing aggregate morphology. Section 3 then applies RDG-FA theory to these aggregates, before Section 4 validates this approach against previous studies, examining the MAC and MSC for different aggregate configurations and performing a sensitivity analysis.

2. Modeling of fractal aggregates

2.1 Fractal aggregates

Fractal objects demonstrate scale invariant symmetry in that they look the same when viewed at different scales. Scientists have long used this concept to describe the structure of aggregates [8]. Forrest and Witten [9] showed that

$$N_p = k_f \left(\frac{2R_g}{d_p} \right)^{D_f}, \quad (1)$$

where N_p is the number of primary particles within the aggregate, d_p is the primary particle diameter, and k_f , D_f and R_g are scaling prefactor, fractal dimension, and radius of gyration of the aggregate, respectively. As per Sorensen [10], this study uses $D_f = 1.78$ and $k_f = 1.3$, which is characteristic of soot, to calculate the optical properties in subsequent

*M.A.Sc Candidate, corresponding author, keyhan.babaee@ubc.ca

•Postdoctoral fellow, tsipkens@mail.ubc.ca

†Professor, principle investigator, rogak@mech.ubc.ca

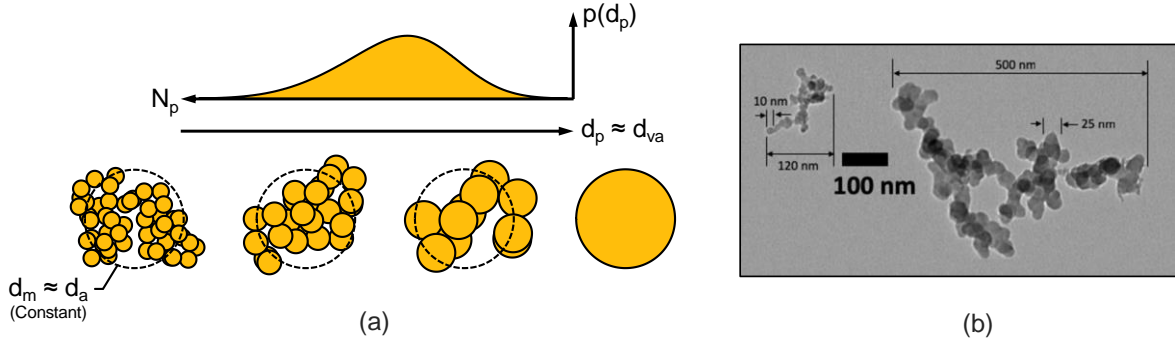


Figure 1. (a) Schematic of the soot aggregates with the same mobility diameter, where d_p , d_{va} , N_p , d_m and d_a are primary particle diameter, Sauter-mean diameter of the primary particle, primary particle number within the aggregate, aggregate mobility diameter and projected area equivalent diameter of the aggregate, respectively. (b) Increase in primary particle size with mobility diameter, TEM image of soot from a non-premixed flame.

sections. We now seek to evaluate the radius of gyration from this expression, which requires further knowledge of N_p and d_p , which we derive from other relations governing the aggregate structure.

2.2 Relationship between the mass and mobility diameter of aggregates

Further information about the structure of the aggregates can be derived from the relationship between the mass and mobility diameter of soot aggregates. These quantities can be determined using tandem measurements that combine any two of (a) mobility classifier, (b) mass classifier, or (c) inertial classifier [11]. This can be complimented by ex situ characterization using transmission electron microscopy (TEM). These kinds of measurements have been used to define an empirical mass-mobility relationship [12],

$$m = k d_m^{D_m}. \quad (2)$$

where m is mass of the aggregate, d_m is the mobility diameter, and k and D_m are mass-mobility prefactor and exponent, respectively. This relationship is often rephrased in terms of the effective density [13],

$$\rho_{\text{eff}} = \frac{m}{\pi d_m^3 / 6} = \left(\frac{6k}{\pi} \right) d_m^{D_m - 3}, \quad (3)$$

where the latter form comes from substitution of Eq. (2). From these relations, if any two of ρ_{eff} , k or D_m are known for a specified d_m , the third can be determined. Usually for different fuels and flames ρ_{eff} and D_m for a mobility diameter of 100 nm are reported ($\rho_{\text{eff},100}$). For non-premixed flames, $\rho_{\text{eff},100}$ and D_m have been determined experimentally [7] and generally range between 450-650 kg/m³ and 2.2-2.8, respectively.

2.3 The conditional primary particle size distribution

The average projected area of a fractal-like aggregate, a_a , is related to the number of primary particles within the aggregate by a power law [14],

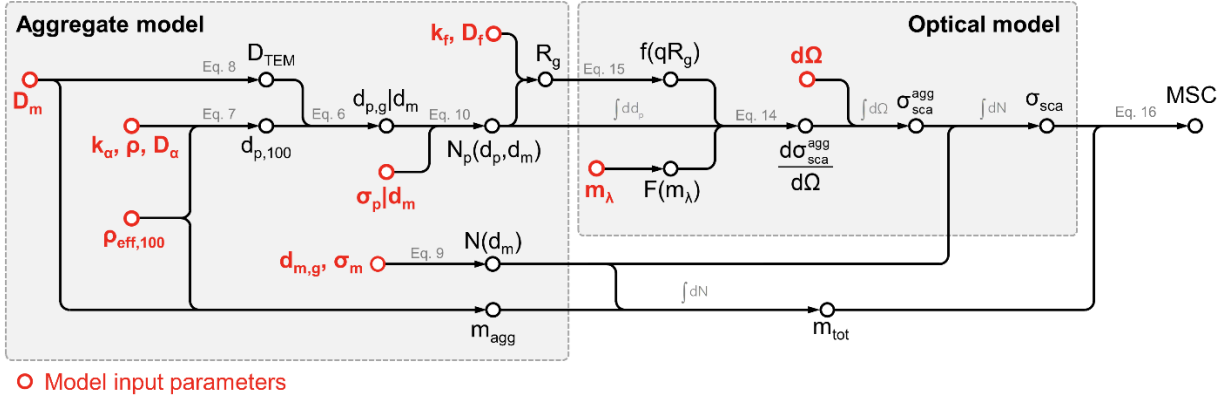
$$n_{va} = k_a \left(\frac{a_a}{a_{va}} \right)^{D_\alpha}, \quad (4)$$

where $a_{va} = \pi d_{va}^2 / 4$ is projected area of the primary particle based on the Sauter-mean diameter of the primary particle, d_{va} , and k_a and D_α are the prefactor and projected area exponent of the aggregate, which depend on the morphology of the aggregate [15].

The mobility diameter of the aggregate, d_m , in the free molecular [16] and transition regime [17] is approximately equal to the projected area equivalent diameter, d_a , of the aggregate, that is $d_m \approx d_a$. Under these conditions, the Sauter-mean diameter of the primary particles can be expressed in terms of the mobility diameter as [7]

$$d_{va}|d_m = \left(\frac{\pi k_a \rho}{6k} \right)^{\frac{1}{2D_\alpha - 3}} (d_m)^{\frac{2D_\alpha - D_m}{2D_\alpha - 3}}, \quad (5)$$

where ρ is the material density of soot. This equation is an empirical relation where the conditional is included to explicitly show that this relation is applied for an aggregate with a specific mobility diameter. Then, by approximating the geometric mean diameter of the primary particles as the Sauter mean diameter, $d_{p,g} \approx d_{va}$, and $\rho = 1800 \text{ kg/m}^3$ [18], this equation can be used to estimate geometric mean primary particle size within the aggregate as a function of the mobility diameter of the aggregate [15], resulting in the summary expression



○ Model input parameters

Figure 2. Schematic demonstrating the procedure of calculating the MSC in the current work, incorporating existing relations for the structure of the aggregates.

$$d_{p,g}|d_m = d_{p,100} \left(\frac{d_m}{100} \right)^{D_{TEM}}, \quad (6)$$

where $D_{TEM} = (2D_\alpha - D_m)/(2D_\alpha - 3)$ and $d_{p,100}$ is primary particle diameter of an aggregate having a mobility diameter of 100 nm. The latter quantity can be derived from

$$d_{p,100} = d_{va,100} = 100 \left(\frac{\rho_{eff,100}}{k_a \rho} \right)^{\frac{1}{3-2D_\alpha}}. \quad (7)$$

where $\rho_{eff,100}$ is obtained by Eq. (3) when $d_m = 100$ nm. Dastanpour [15] found that $D_\alpha \approx 1.1$ and $k_a \approx 1.13$, such that

$$D_{TEM} = 1.25D_m - 2.75. \quad (8)$$

We note that, if $D_m = 2.2$, then $D_{TEM} = 0$, which is the same value that Sorensen [10] recommended as the normal for the transition regime for fractal aggregate with constant primary particle size.

Lastly, Dastanpour and Rogak [19] showed that aggregates sharing a mobility diameter have a lognormal primary particle distribution with geometric mean $d_{p,g}$ and geometric standard deviation $\sigma_p|d_m$. Dastanpour and Rogak also demonstrated that primary particle sizes within an aggregate don't change significantly, such that the distribution width instead manifests in different numbers of particles with aggregates of a given mobility diameter.

2.4 The mobility diameter distribution

Finally, the distribution of the mobility diameter is traditionally assumed to be lognormal [20],

$$\frac{dN}{d \ln d_m} = \frac{N_{tot}}{(2\pi)^{0.5} \ln \sigma_g} \exp \left[-\frac{(\ln d_p - \ln d_{m,g})^2}{2 \ln^2 \sigma_g} \right] \quad (9)$$

where N_{tot} is the total number concentration of particles, $d_{m,g}$ and σ_g are geometric mean diameter and geometric standard deviation of the mobility diameter distribution, respectively.

2.5 Programming

A program was developed by the authors to consider these properties, discretizing the space of feasible mobility and primary particle diameters. An appropriate discretization was chosen to ensure grid independence. Within this program, D_m and $\rho_{eff,100}$ are specified as model inputs such that k can be evaluated. We also specify D_m as a model input such that D_{TEM} can be determined using Eq. (8). Then, for a given mobility diameter, the geometric mean diameter of the primary particle ($d_{p,g}|d_m$) can then be calculated using ρ , $d_{p,100}$, and Eq. (6). Using a constant value of $\sigma_p|d_m$ and $d_{p,g}|d_m$, one can determine the probability of encountering an aggregate with primary particle size (d_p) for a given aggregate mobility diameter (d_m). Eq. (4) can now be used to define the number of primary particles within aggregates of a specified d_p and d_m as

$$N_p = 1.13 \left(\frac{d_m}{d_p} \right)^{2.2}, \quad (10)$$

where $N_p \approx n_{va}$ is the number of primary particles within each aggregate. The remaining parameter, the radius of gyration from Eq. 1, can finally be determined since N_p , d_p , k_f , and D_f are known. This overall procedure, and the interface with the optical model of Section 3 that allows calculation of the MSC, is shown schematically in Fig. 2.

3. Modeling the optical properties of fractal aggregates

3.1 Rayleigh-Debye-Gans Fractal Aggregate (RDG-FA) Theory

The validity of RDG-FA theory, which neglects multiple scattering between primary particles, is based on two assumptions [5]:

$$|m_\lambda - 1| \ll 1 \quad (11)$$

and

$$2x_p|m_\lambda - 1| \ll 1, \quad (12)$$

where $m_\lambda = n + jk$ is the complex index refraction of the particle material and $x_p = \pi d_p/\lambda$ is the size parameter. Mulholland [21] showed that, for $D_f < 2$, RDG-FA can reasonable predict the optical characteristics of soot aggregates. In this theory, the absorption cross-section is given by [22]

$$\begin{aligned} \sigma_{abs}^p &= 4\pi k_\lambda \left(\frac{d_p}{2}\right)^3 E(m_\lambda) \\ \sigma_{abs}^{agg} &= N_p \sigma_{abs}^p, \end{aligned} \quad (13)$$

for the primary particle and aggregate, respectively; and the differential scattering cross-section is given by

$$\begin{aligned} \frac{d\sigma_{sca}^p}{d\Omega} &= k_\lambda^4 \left(\frac{d_p}{2}\right)^6 F(m_\lambda) \\ \frac{d\sigma_{sca}^{agg}}{d\Omega} &= N_p^2 \frac{d\sigma_{sca}^p}{d\Omega} f(qR_g) \end{aligned} \quad (14)$$

where Yang and Köylü [23] introduced the shape factor

$$f(qR_g) = \left[1 + \frac{8(qR_g)^2}{3D_f} + (qR_g)^8 \right]^{-D_f/8}, \quad (15)$$

$k_\lambda = 2\pi/\lambda$ is the wave number, $E(m) = \text{Im}[(m_\lambda^2 - 1)/(m_\lambda^2 + 2)]$ is the absorption function, and $F(m) = |(m_\lambda^2 - 1)/(m_\lambda^2 + 2)|^2$. The modulus of the scattering vector, $q = 2k_\lambda \sin(\theta/2)$, and solid angle, Ω , will be used to calculate the scattering cross section over a certain area of interest. The total scattering by an aggregate is determined by integrating the differential scattering over solid angle. The average absorption and scattering cross section of a particle with a given mobility diameter is found by integrating over the primary particle size distribution, conditional on a specified mobility diameter.

3.2 Calculating the MSC using RDG-FA

Next, a second integration is then performed over the distribution of mobility diameters to determine the MSC,

$$MSC = \frac{\int_l^u \sigma_{sca}^{agg} dN}{\int_l^u m_{agg} dN}, \text{ where } u = d_{m,g}(\sigma_g)^n, l = d_{m,g}(\sigma_g)^{-n} \quad (16)$$

where $n = 3$ corresponds to integrating over three geometric standard deviations from the geometric mean in both directions.

4. Model Validation and its dependencies on aggregate morphology

The present model is validated against the work of Liu and Snelling [24], for the refractive index of 1.6+0.6j at $\lambda = 532$ nm and $\lambda = 1064$ nm with constant primary particle size equals to 30 nm. We briefly note that the mass-absorption coefficient (MAC) predicted by RDG-FA only depends on the refractive index and wavelength, such that the quantity is insensitive to the parameters of interest to this study. While, Bond and Bergstrom [25] suggest a MAC of 7.5 m²/g for the black carbon with the refractive index of 1.95+0.79j at 550 nm, our result of 4.85 m²/g is consistent with the value that Forestieri et al. [6] determined from RDG-FA (4.9 m²/g), suggesting remaining inadequacies in RDG-FA theory.

4.1 Dependence of the MSC on the mobility and primary particle distributions

As the MSC is insensitive to the number concentration (it cancels out in the relevant equations), we instead vary the refractive index over two different wavelengths, specifically those given by Bond and Bergstrom [25] and Liu and Snelling [24]. For each refractive index, ten cases are considered. In six of the cases, the sample properties ($d_{m,g}$, σ_g)

remained constant and D_m , $\rho_{eff,100}$ and $\sigma_p|d_m$ are varied. The remaining cases vary the aggregate size distribution parameters. This is repeated for both values of the refractive index.

Fig. 3a shows how the MSC changes with mobility diameter. The results show that increase in the primary particle polydispersity ($\sigma_p|d_m$) from 1.0 to 1.4 causes the MSC to increase by up to 17% for aggregates of the same $\rho_{eff,100}$ and D_m . This is a consequence of the primary particle polydispersity being applied to each aggregate mobility bin, where the assumption allows one to consider aggregates with higher scattering cross-sections at the same aggregate mobility diameter by increasing $\sigma_p|d_m$.

The results also demonstrate that an increase in D_m and $\rho_{eff,100}$ is associated with an increase in the MSC. The MSC increases when the aggregate size distributions parameters, $d_{m,g}$ and σ_g increase.

5. Primary particle median diameter

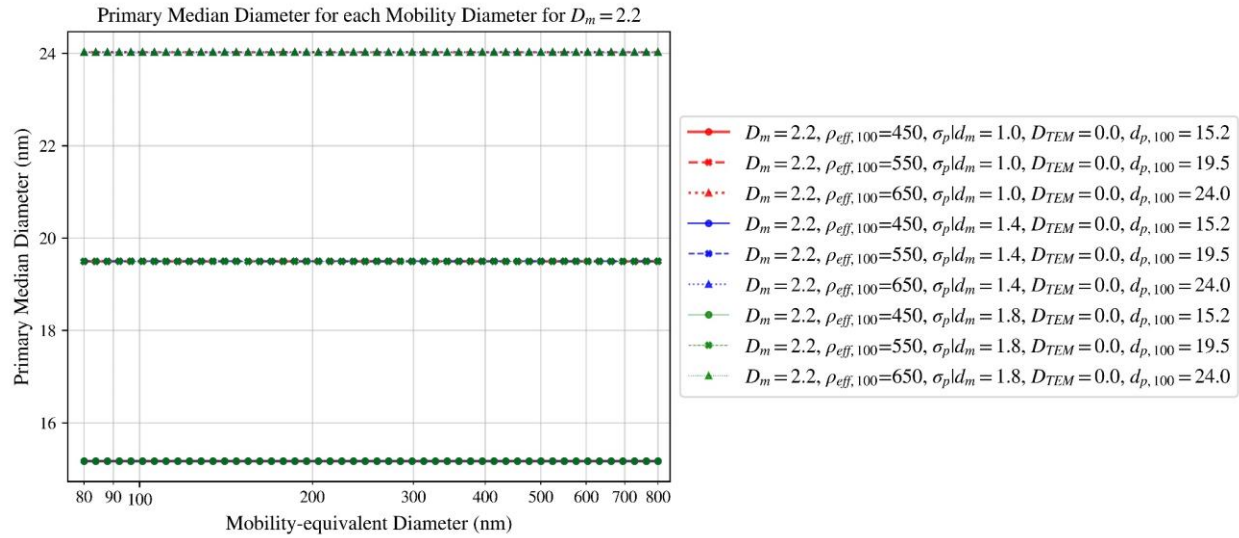


Figure 3

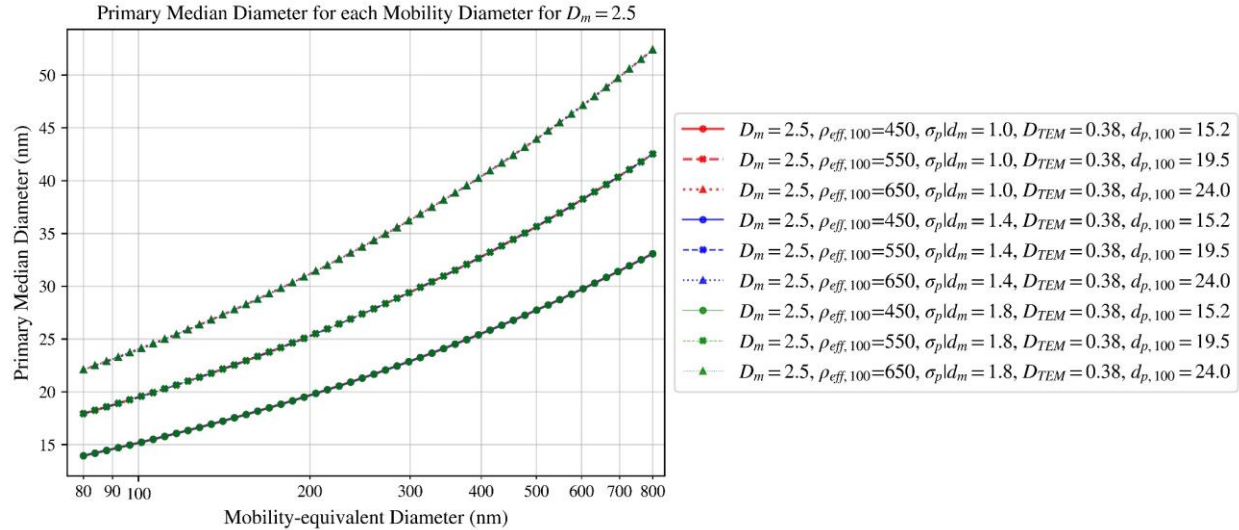


Figure 4

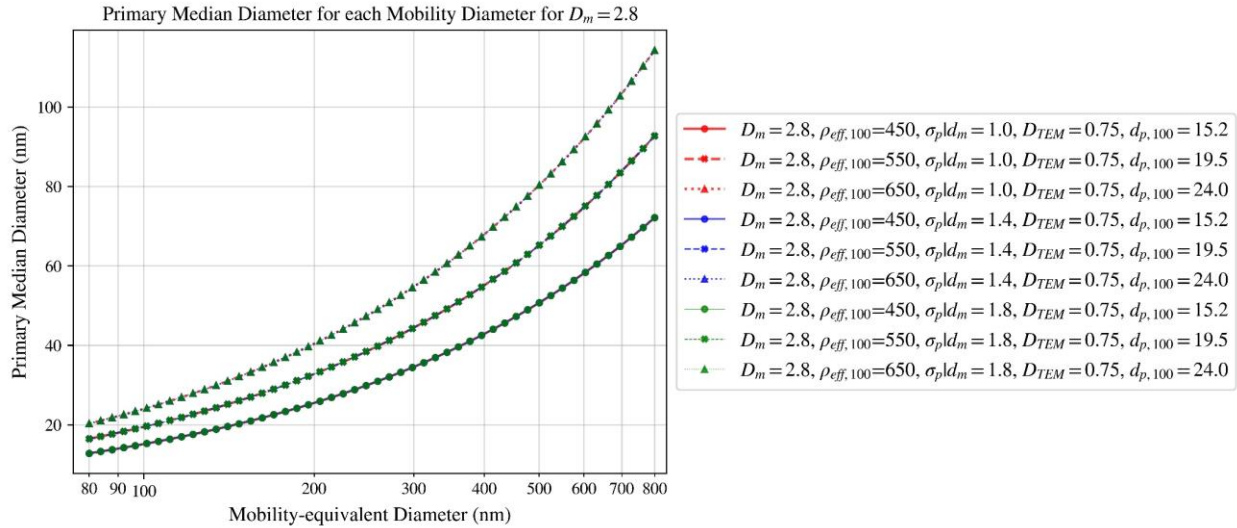


Figure 5

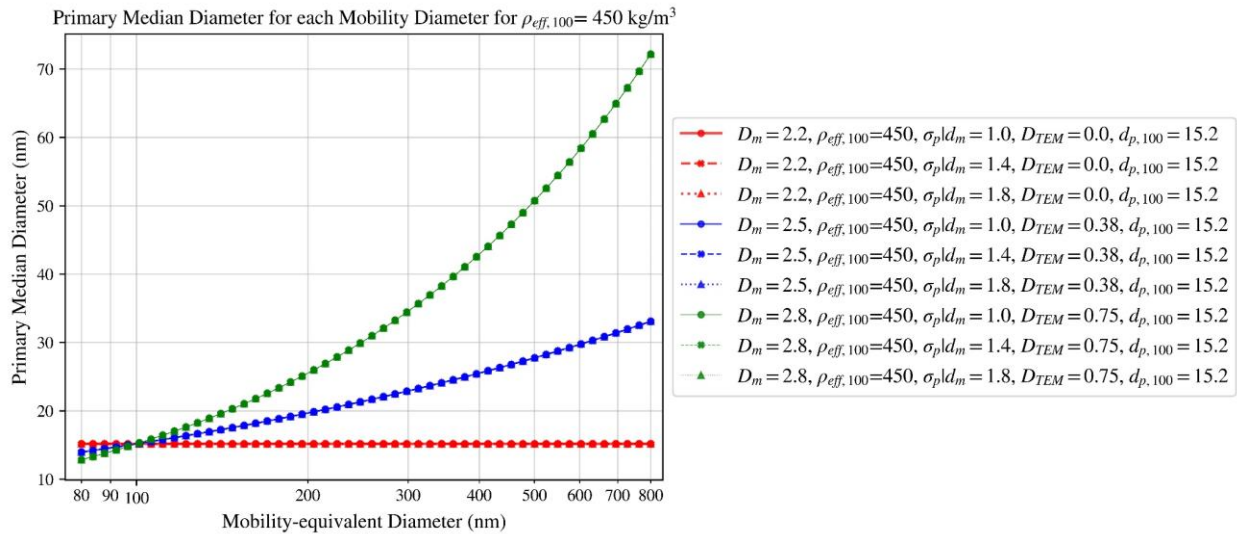


Figure 6

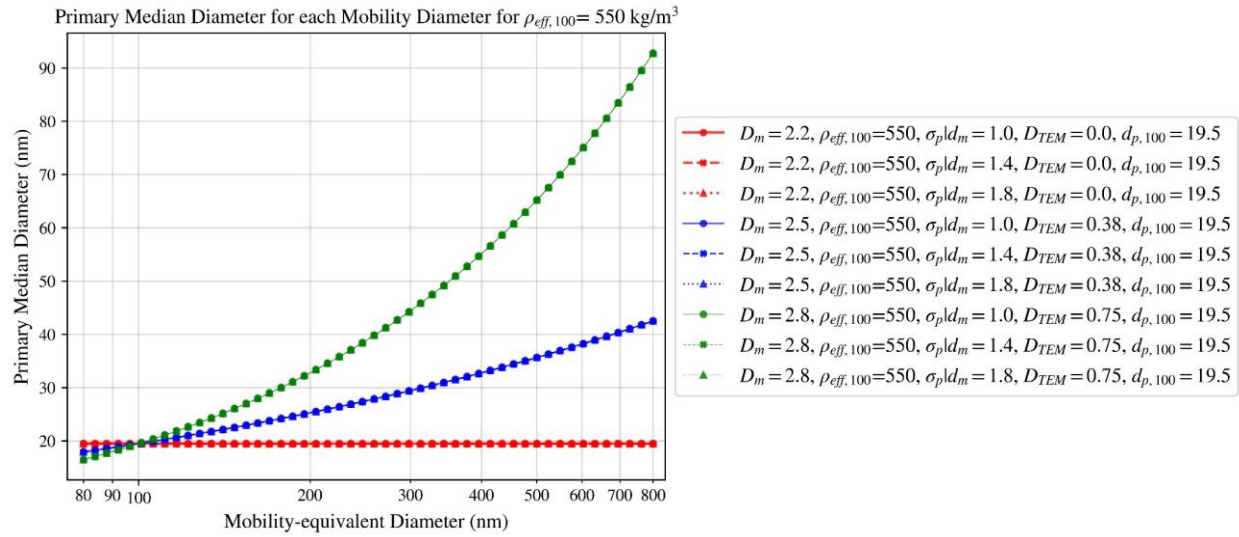


Figure 7

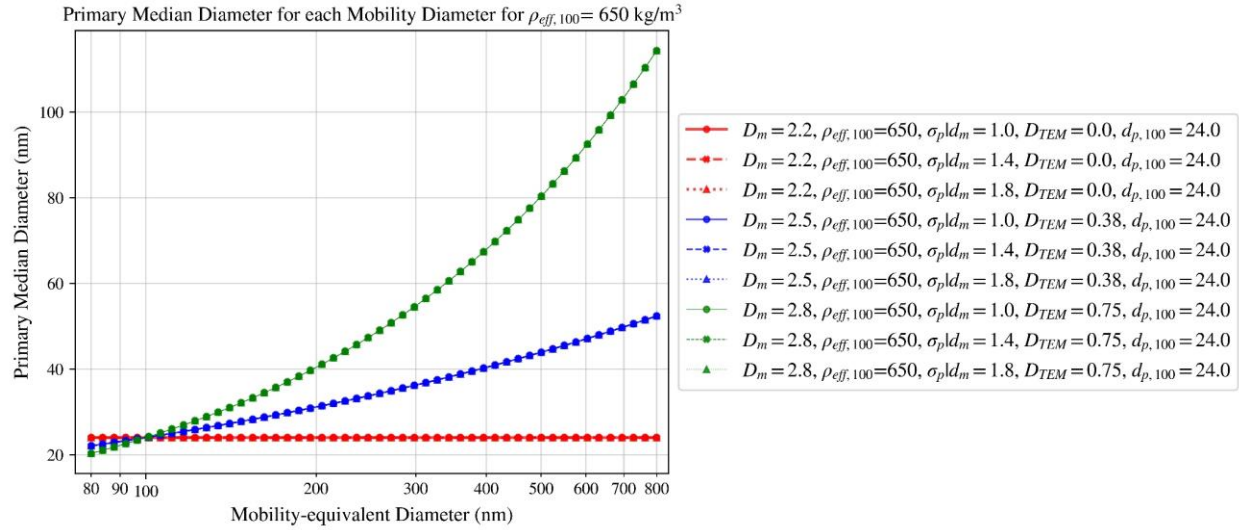


Figure 8

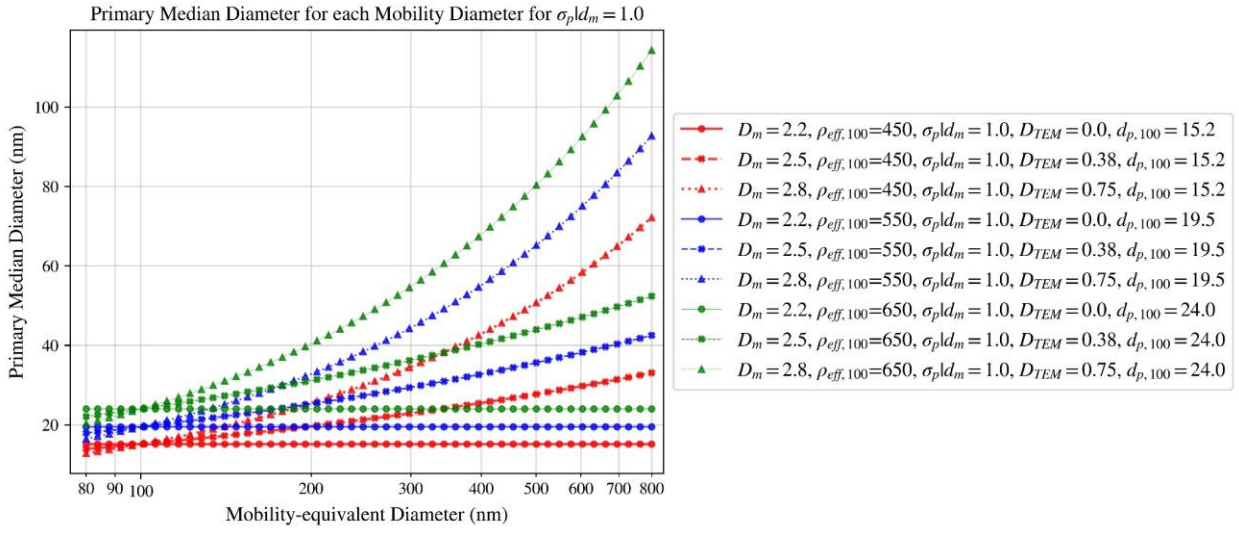


Figure 9

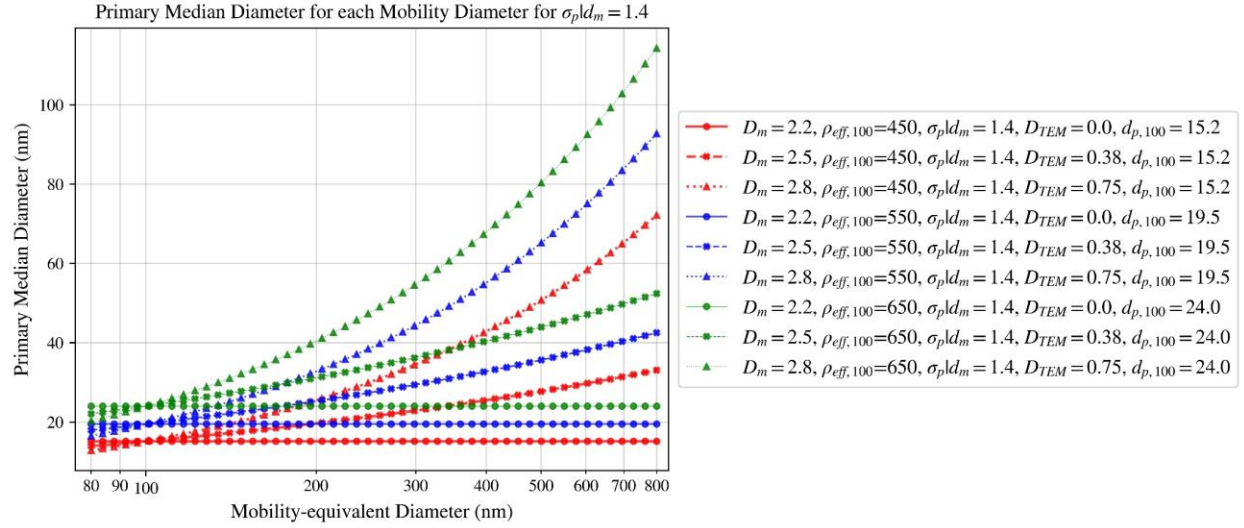


Figure 10

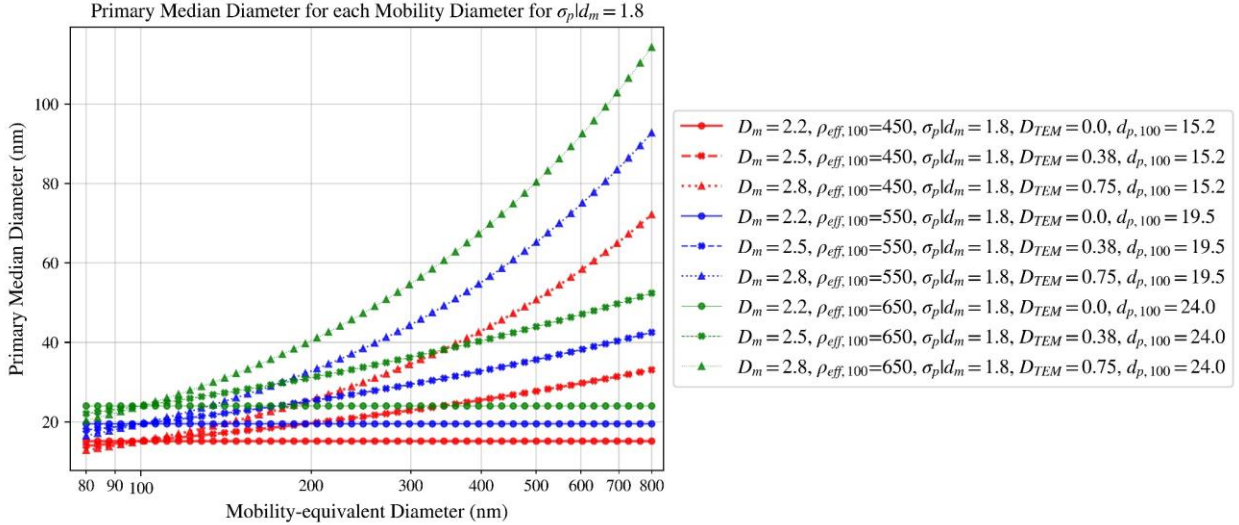


Figure 11

6. RDG-FA absorption and scattering cross-section

?????

7. T-matrix absorption and scattering cross-section

?????

8. RDG-FA single scattering albedo (SSA)

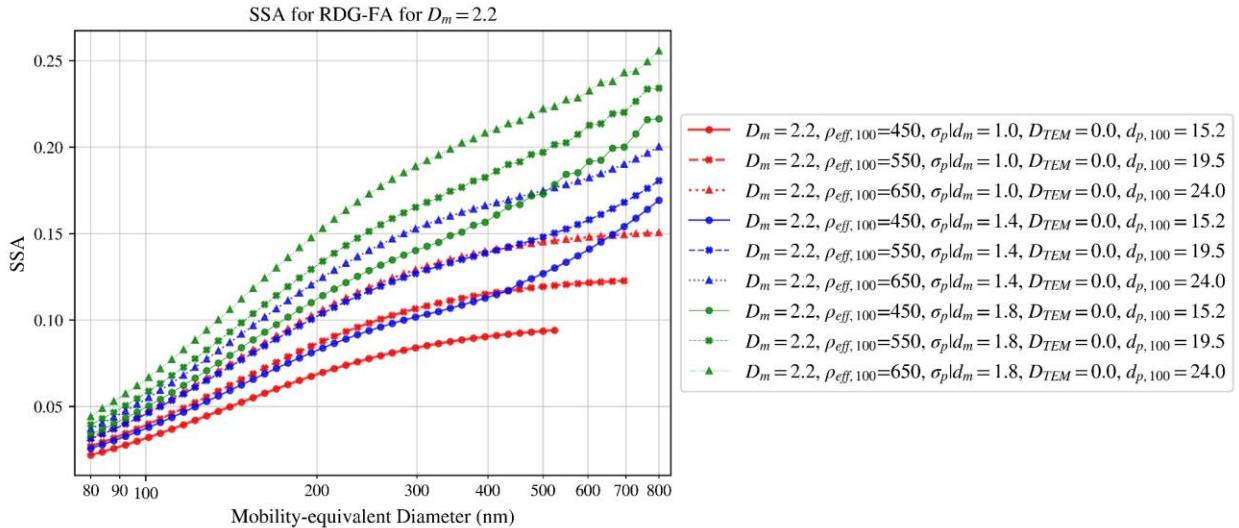


Figure 12

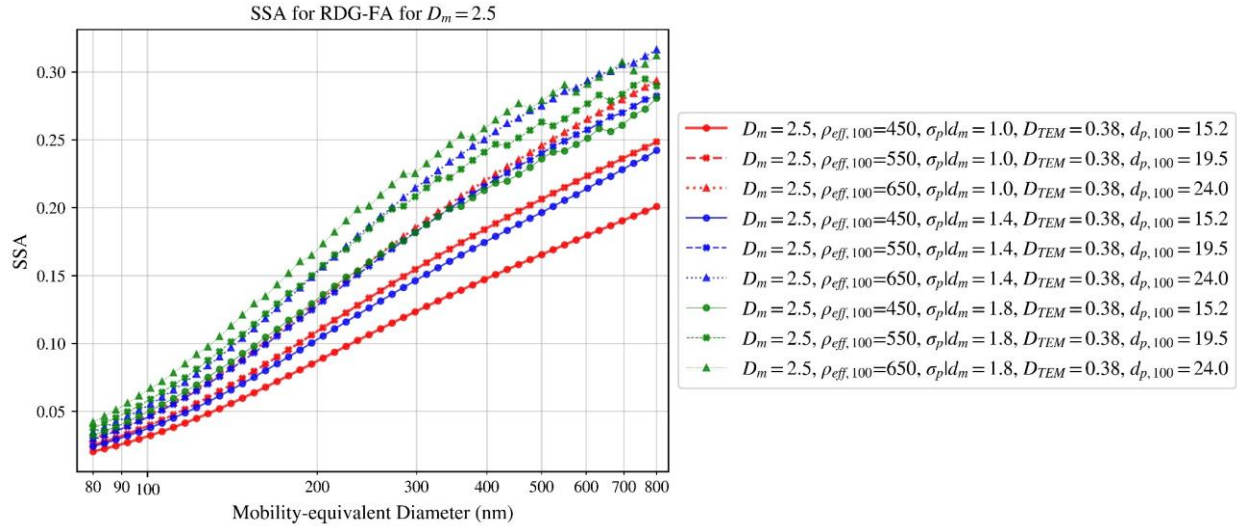


Figure 13

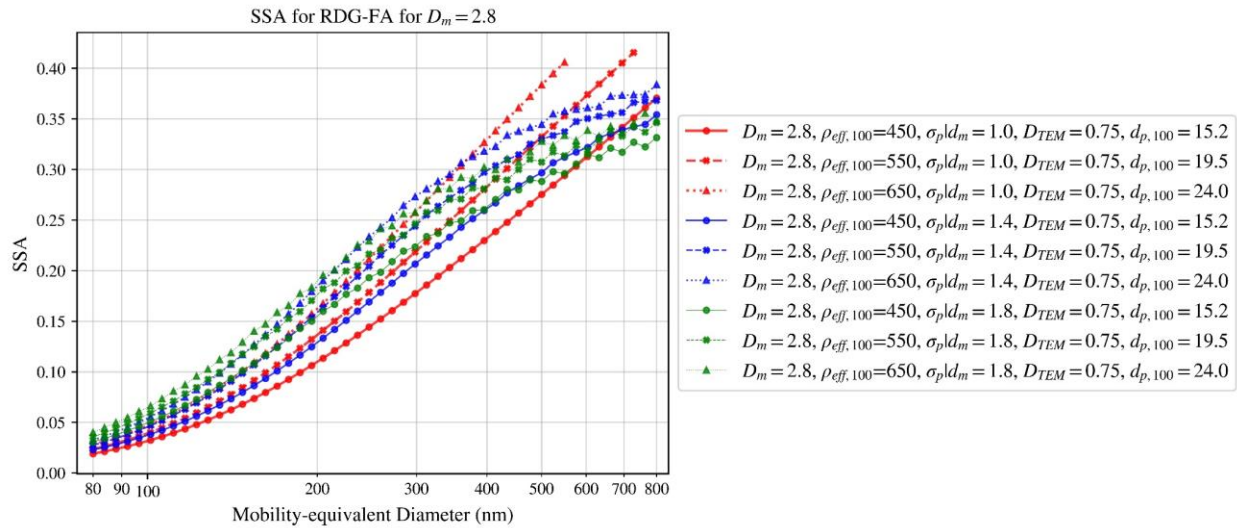


Figure 14

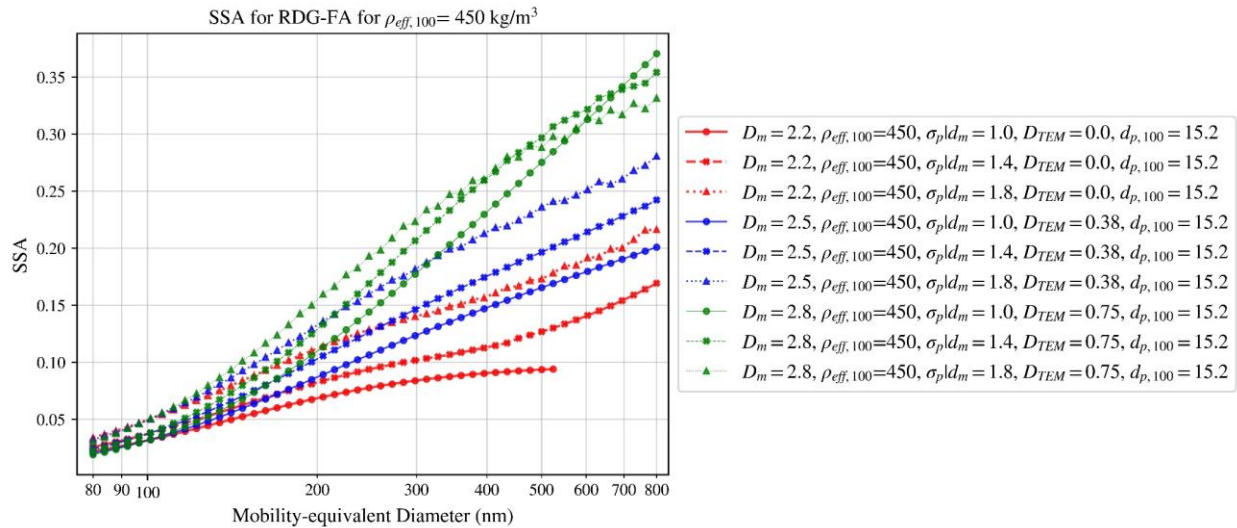


Figure 15

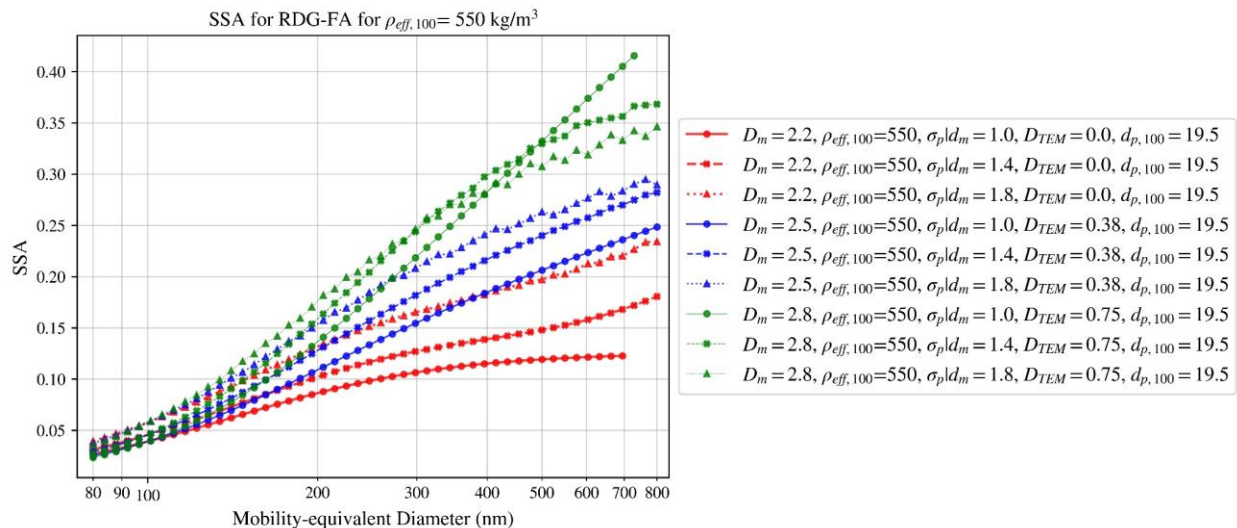


Figure 16

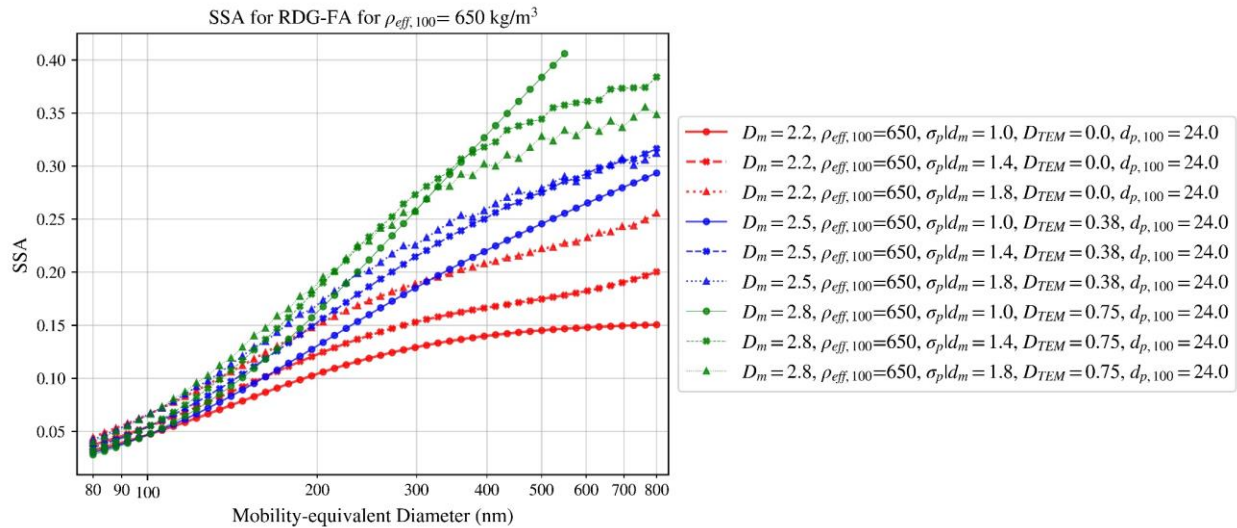


Figure 17

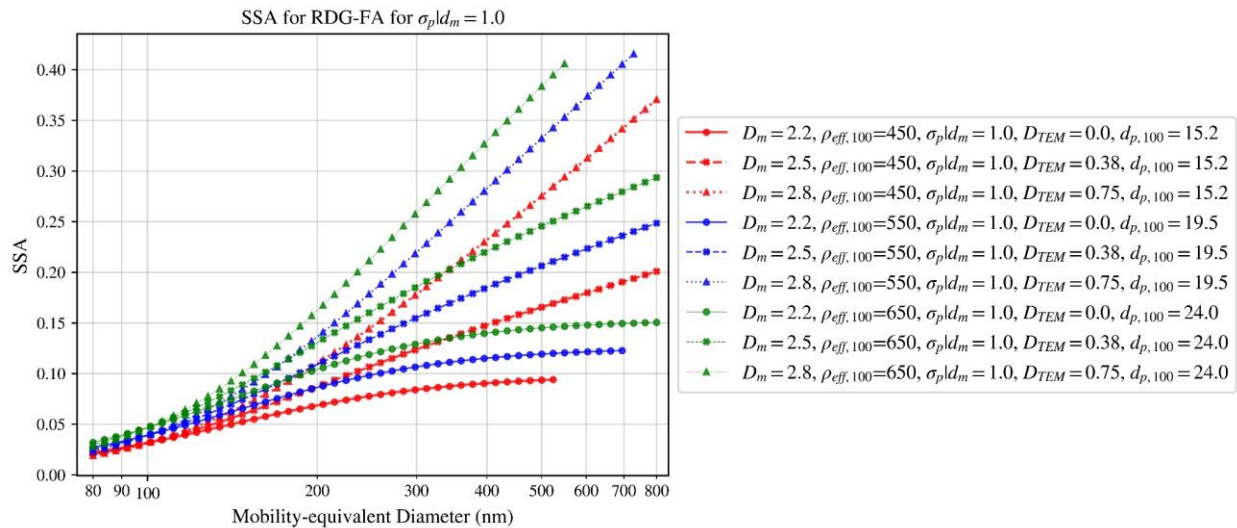


Figure 18

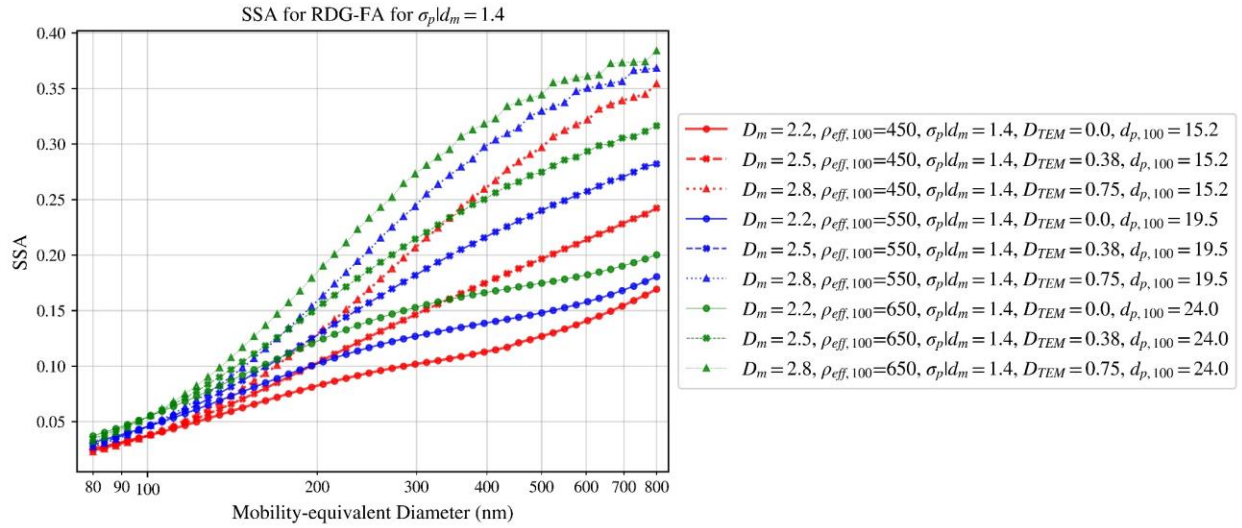


Figure 19

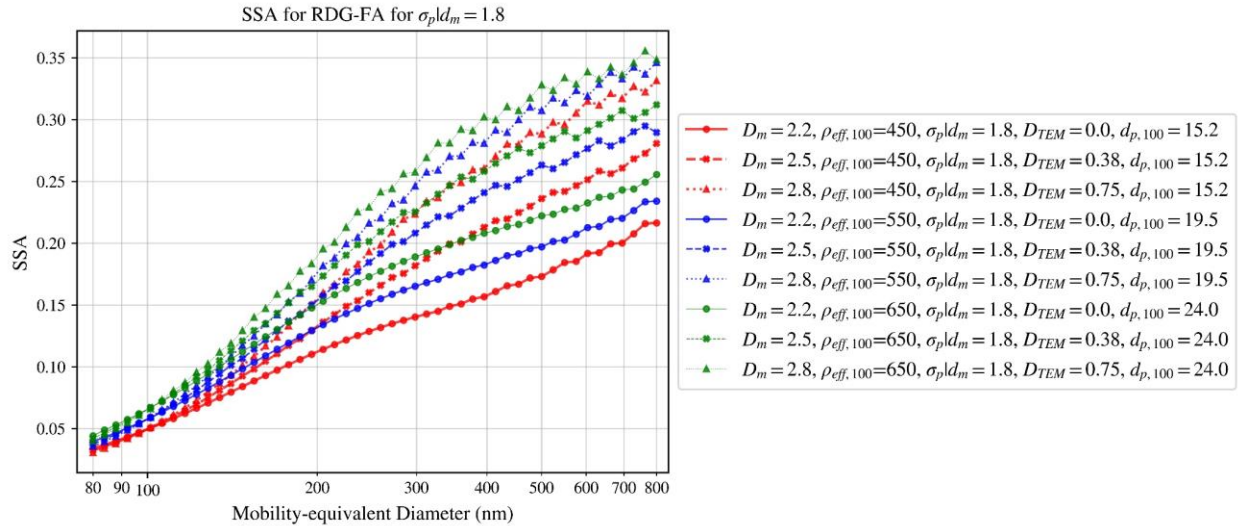


Figure 20

9. T-matrix single scattering albedo (SSA)

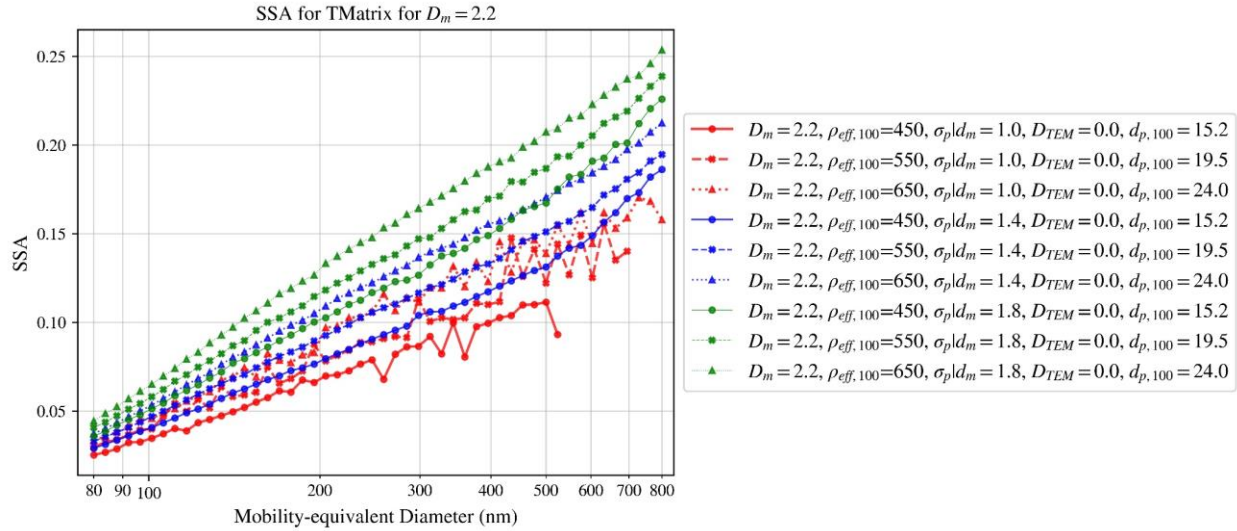


Figure 21

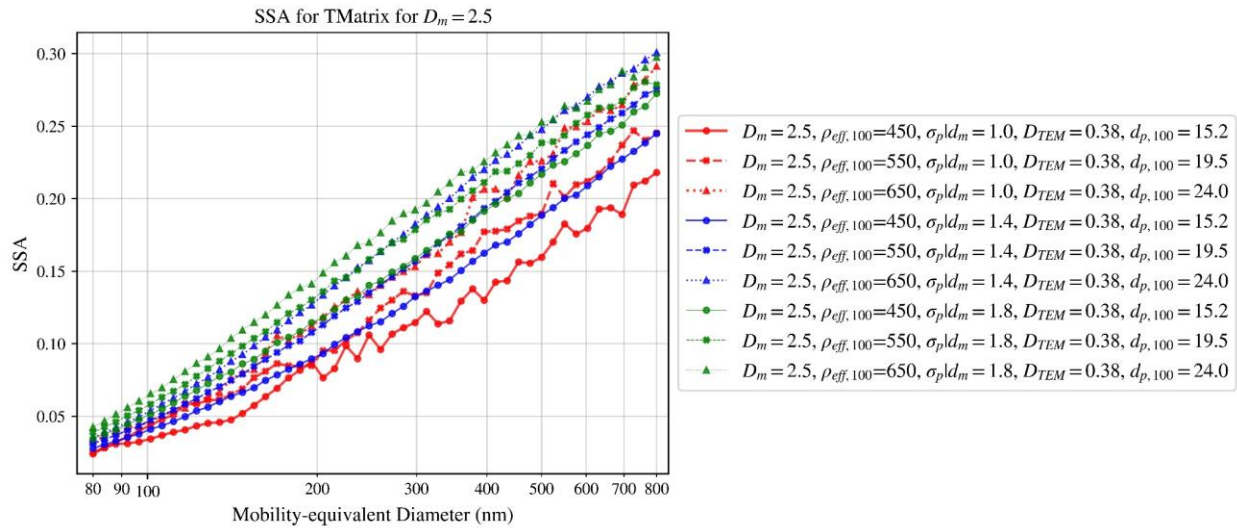


Figure 22

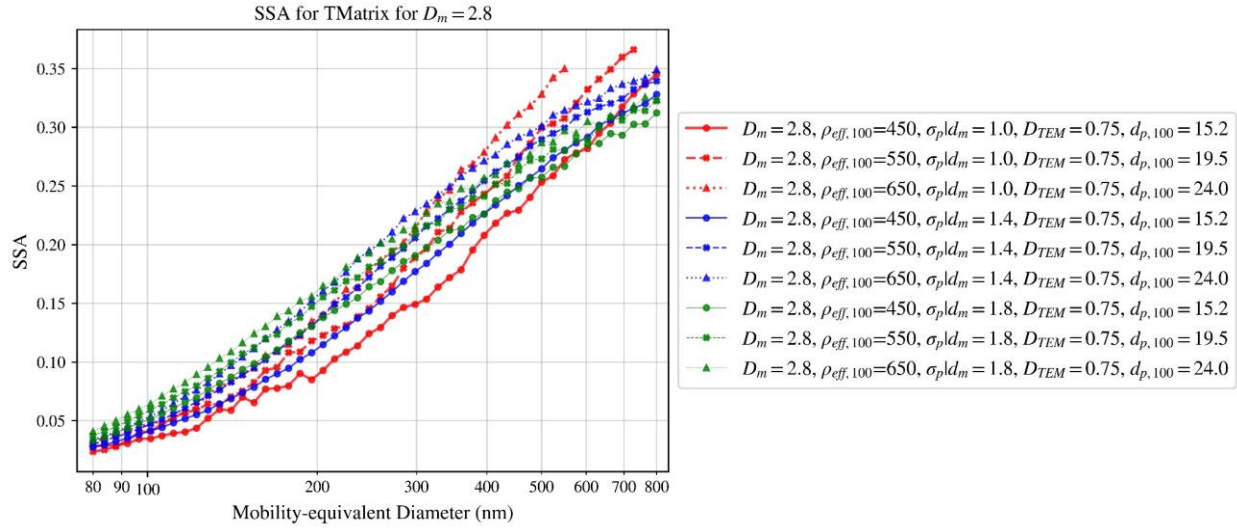


Figure 23

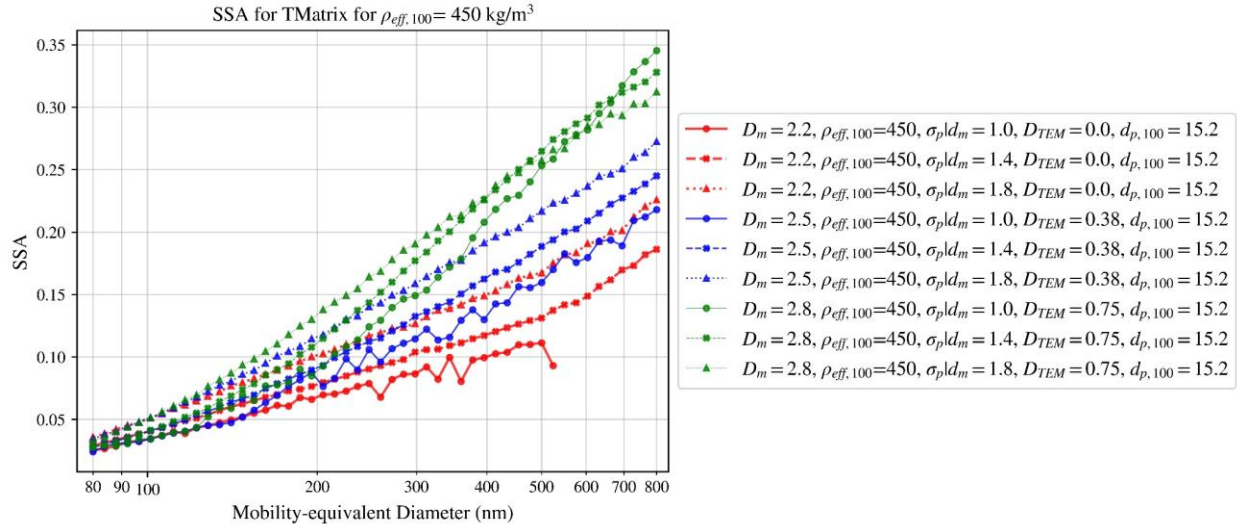


Figure 24

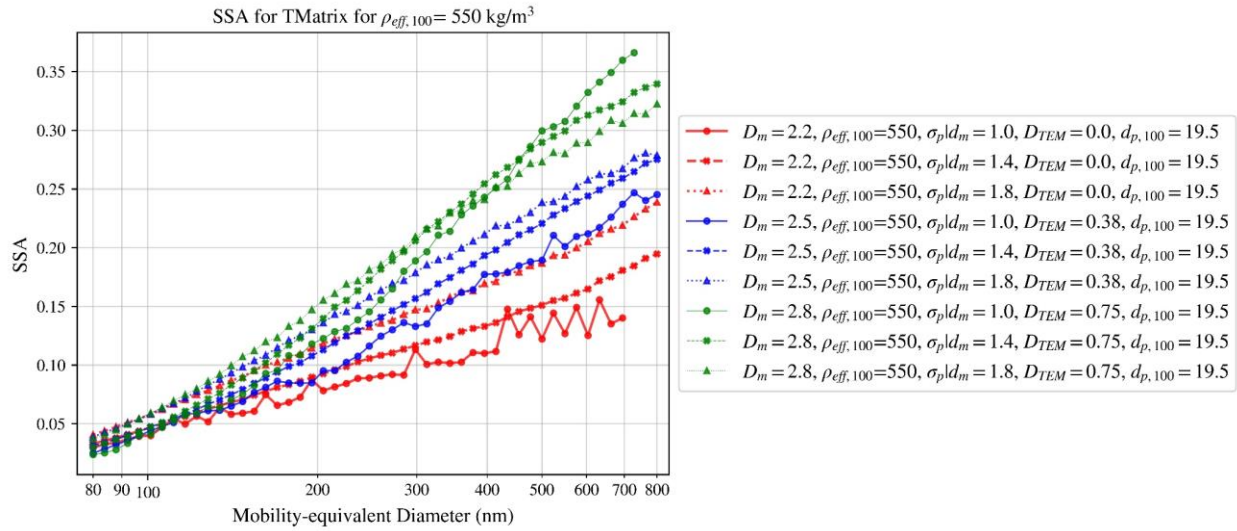


Figure 25

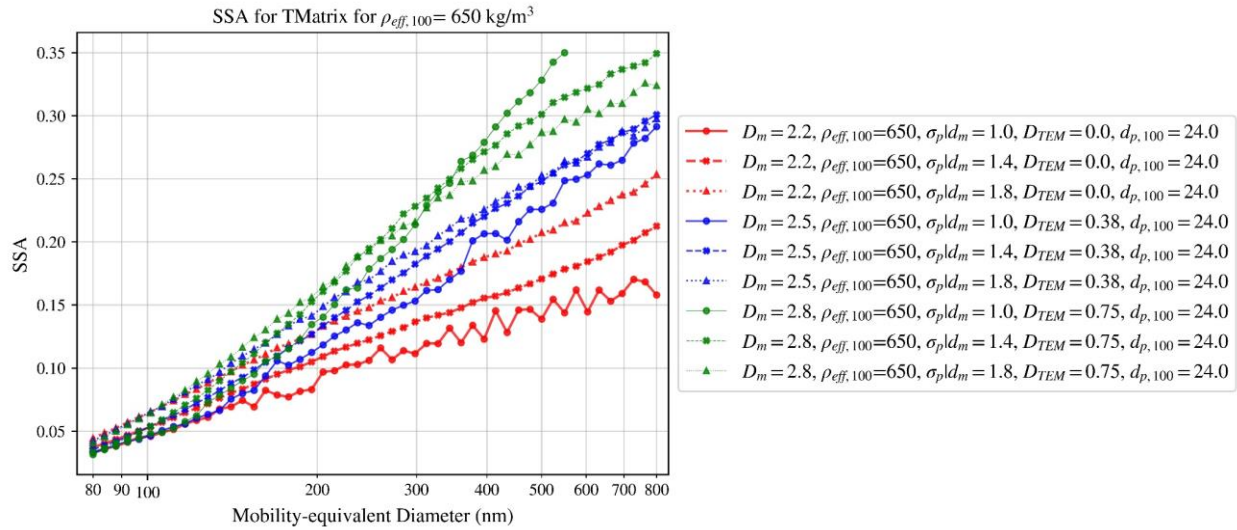


Figure 26

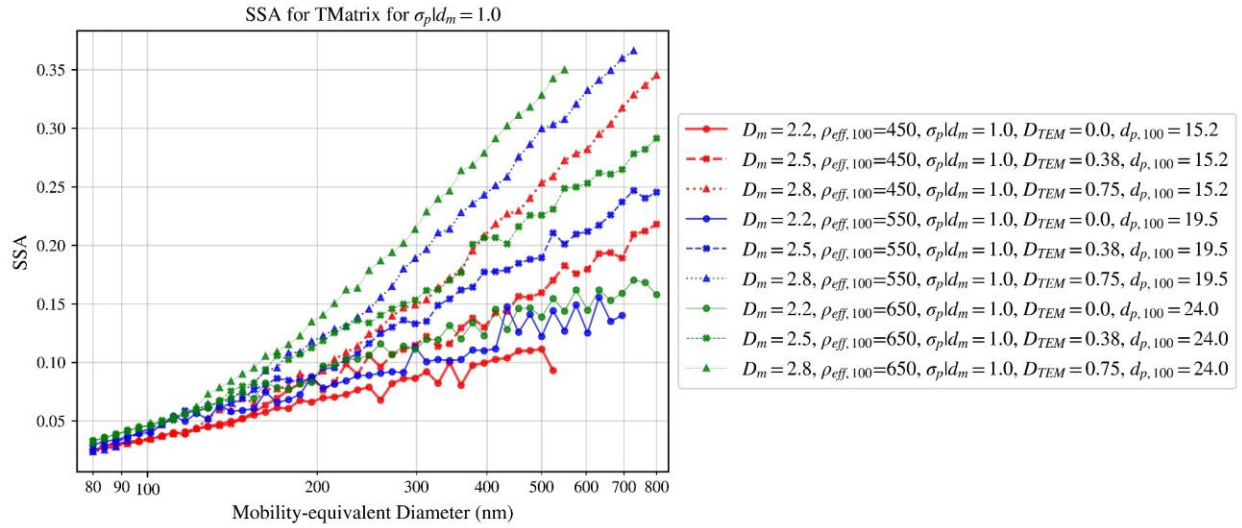


Figure 27

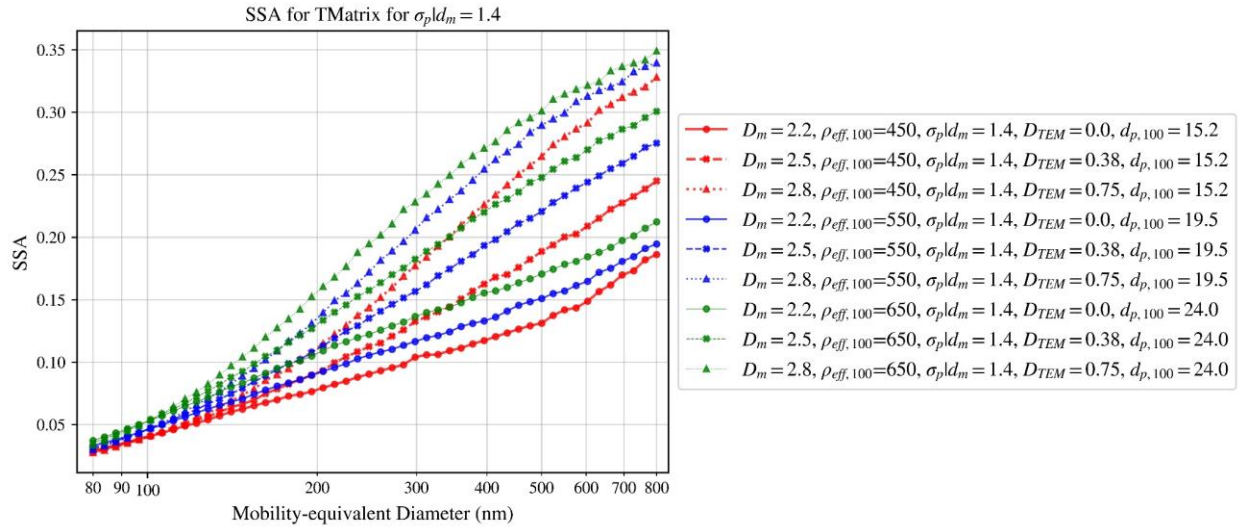


Figure 28

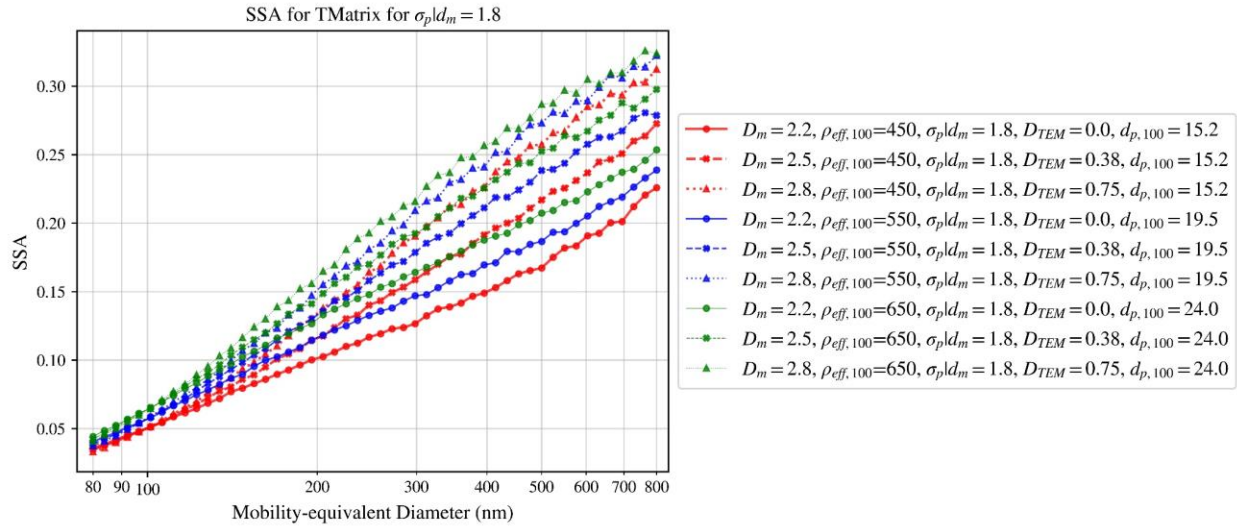


Figure 29

10. T-matrix and RDG-FA absorption cross-section difference

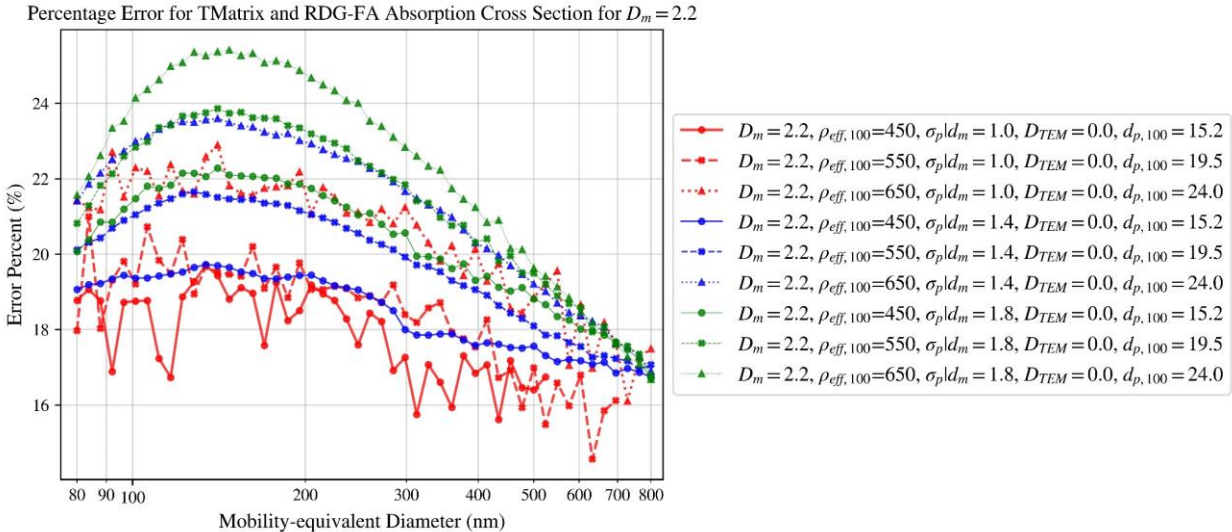


Figure 30

Percentage Error for TMatrix and RDG-FA Absorption Cross Section for $D_m = 2.5$

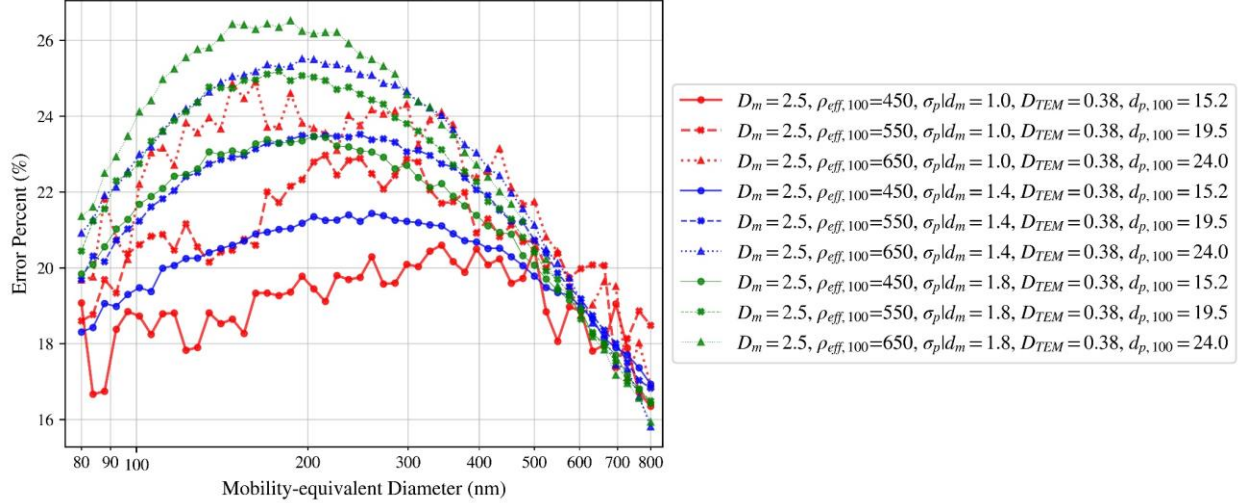


Figure 31

Percentage Error for TMatrix and RDG-FA Absorption Cross Section for $D_m = 2.8$

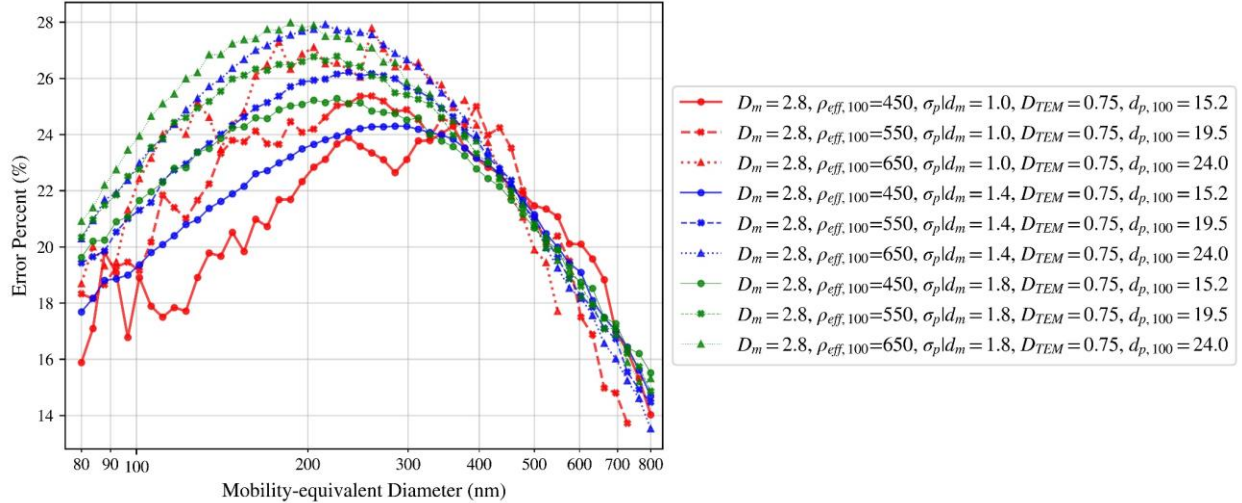


Figure 32

Percentage Error for TMATRIX and RDG-FA Absorption Cross Section for $\rho_{eff,100} = 450 \text{ kg/m}^3$

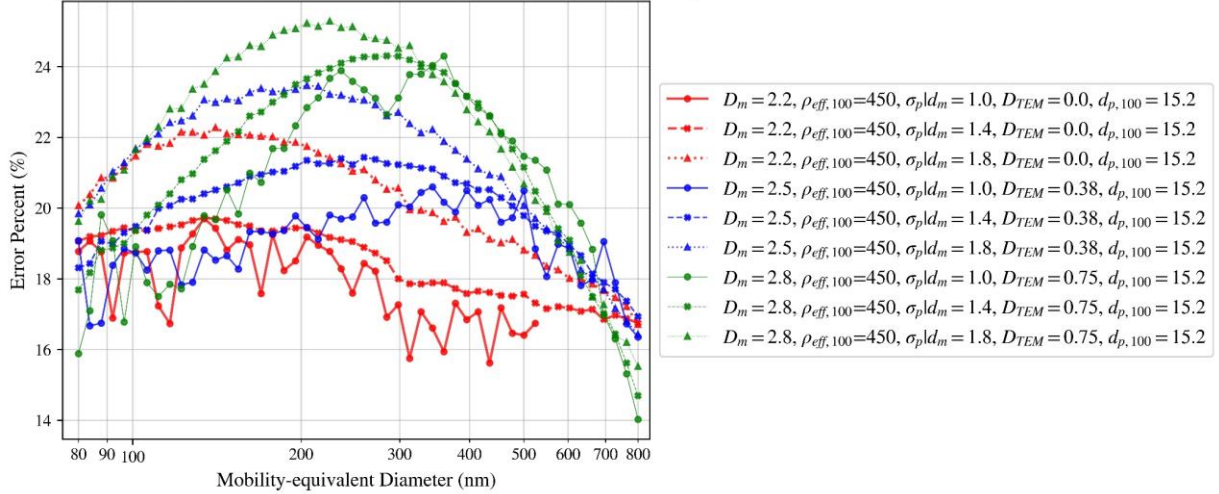


Figure 33

Percentage Error for TMATRIX and RDG-FA Absorption Cross Section for $\rho_{eff,100} = 550 \text{ kg/m}^3$

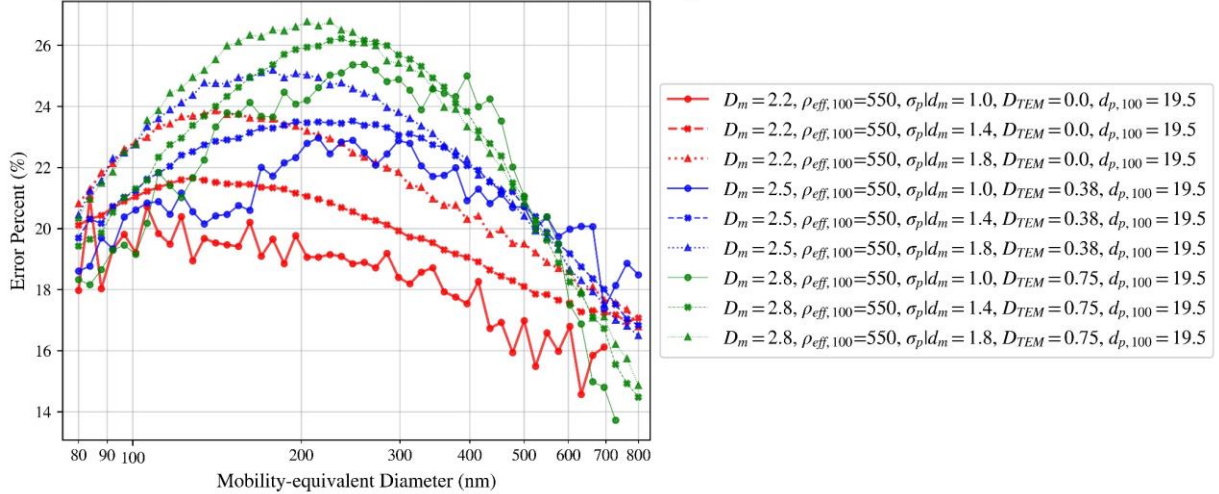


Figure 34

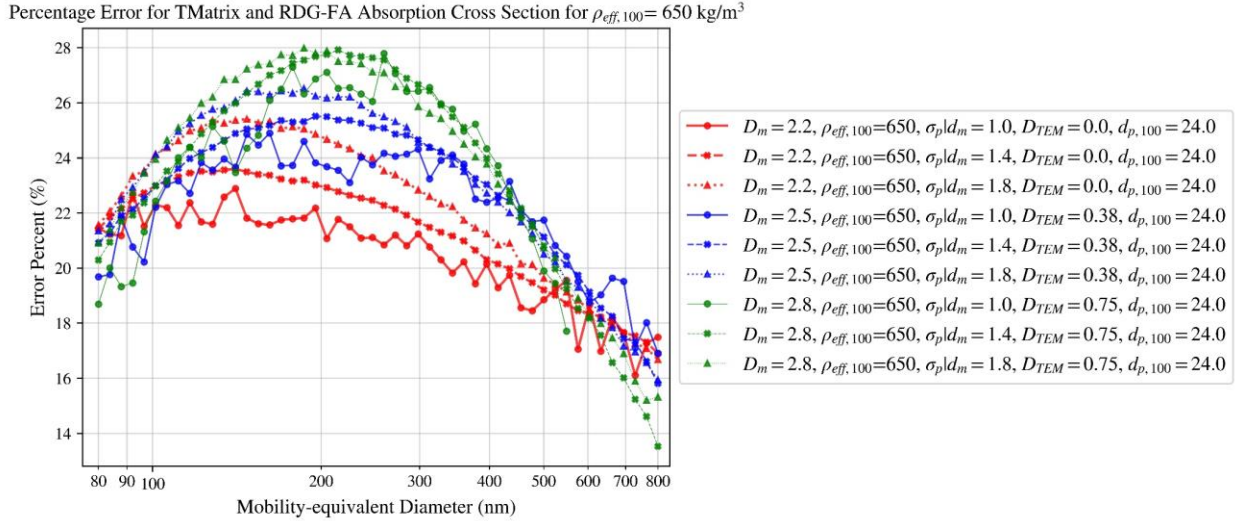


Figure 35

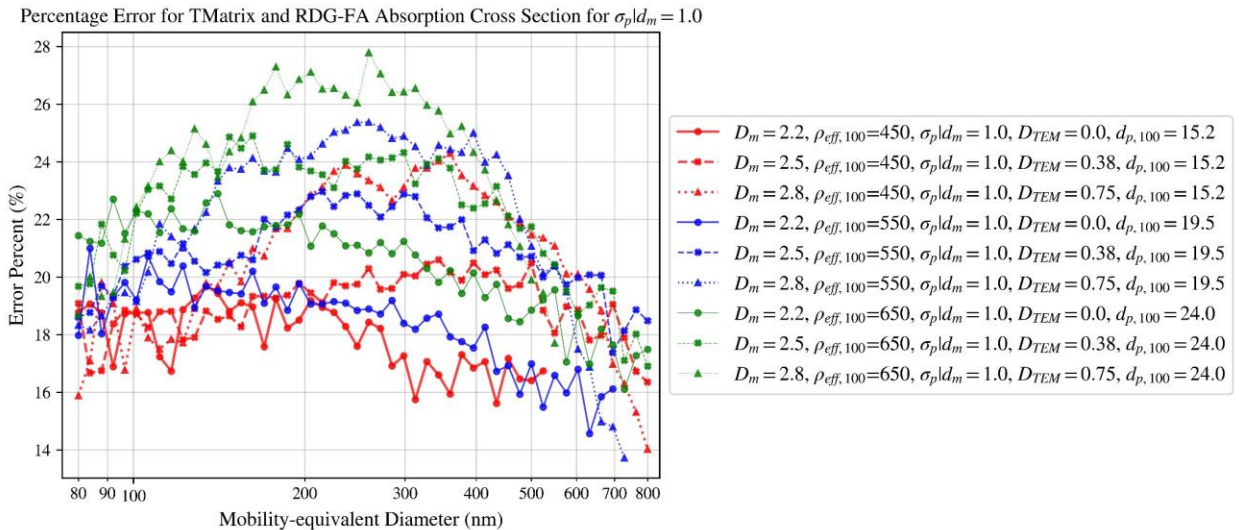


Figure 36

Percentage Error for TMatrix and RDG-FA Absorption Cross Section for $\sigma_p|d_m = 1.4$

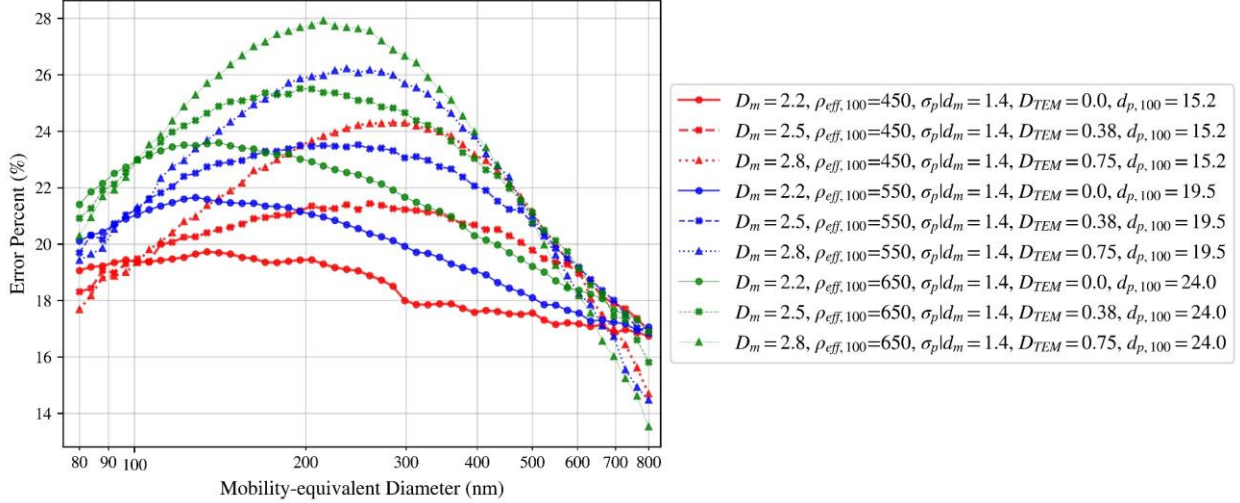


Figure 37

Percentage Error for TMatrix and RDG-FA Absorption Cross Section for $\sigma_p|d_m = 1.8$

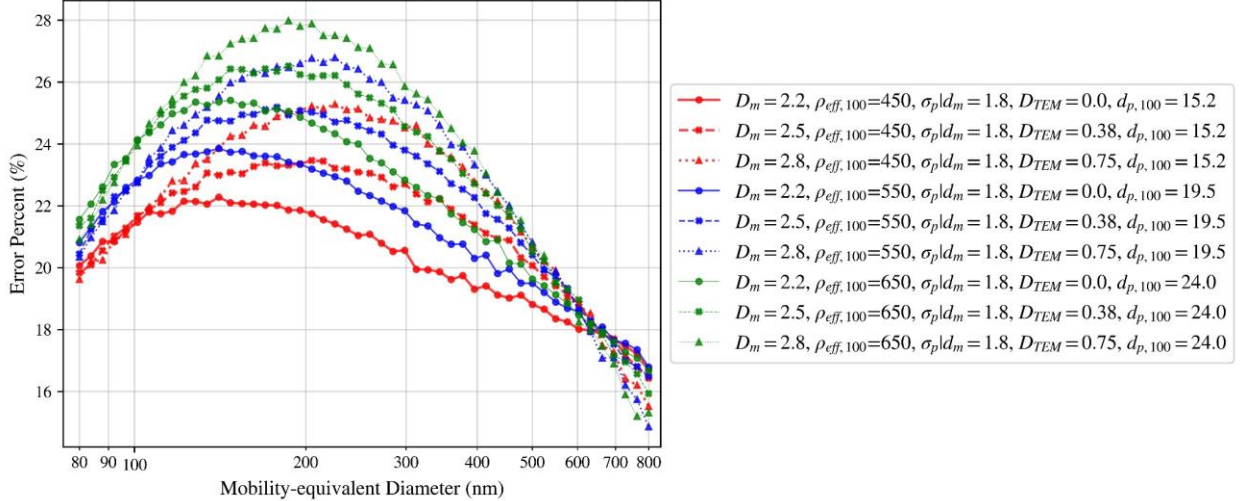


Figure 38

11. T-matrix and RDG-FA scattering cross-section difference

Percentage Error for TMatrix and RDG-FA Scattering Cross Section for $D_m = 2.2$

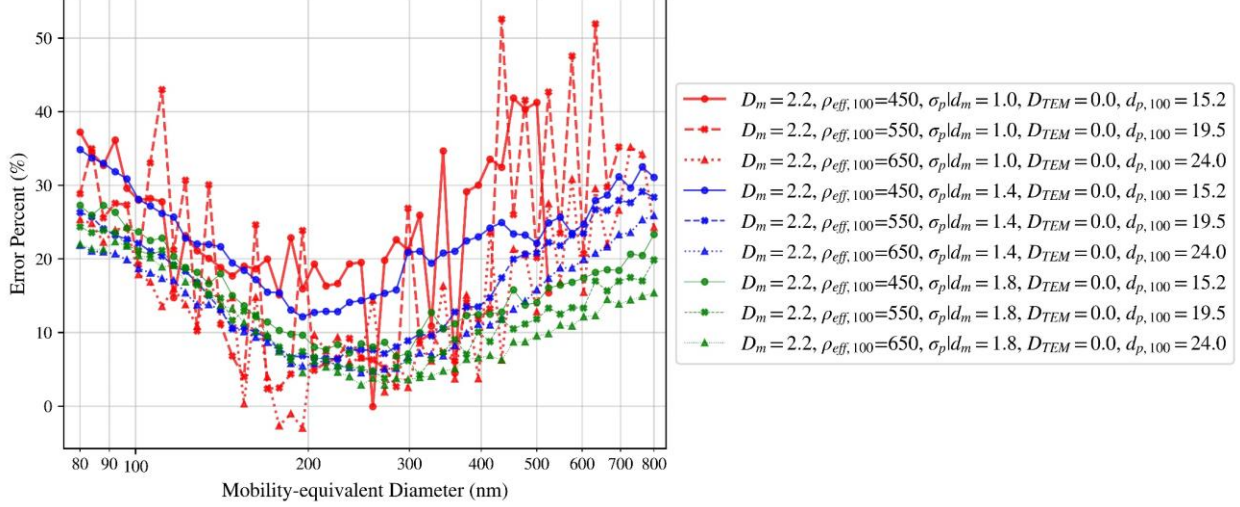


Figure 39

Percentage Error for TMatrix and RDG-FA Scattering Cross Section for $D_m = 2.5$

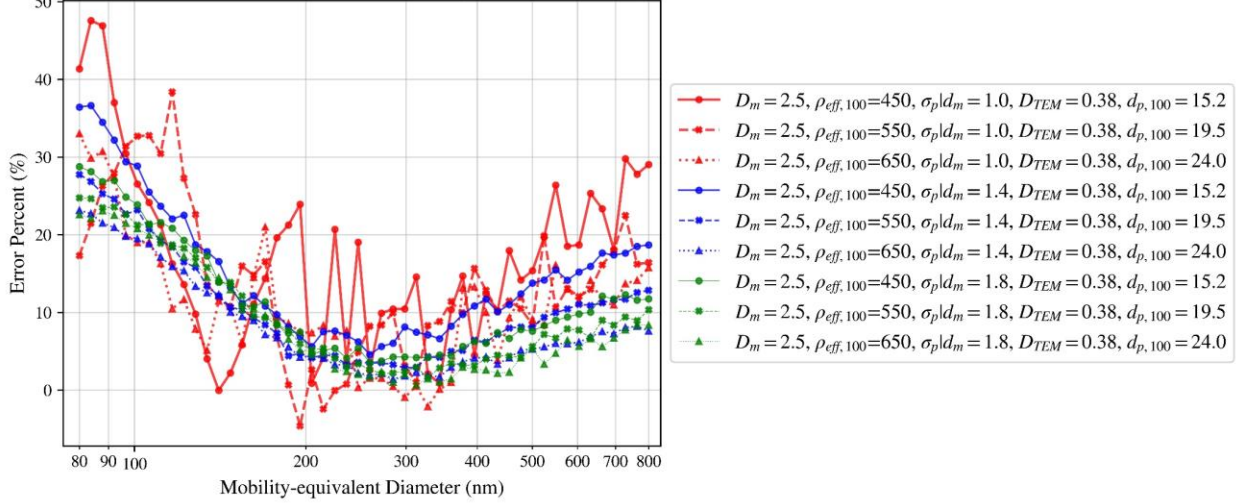


Figure 40

Percentage Error for TMatrix and RDG-FA Scattering Cross Section for $D_m = 2.8$

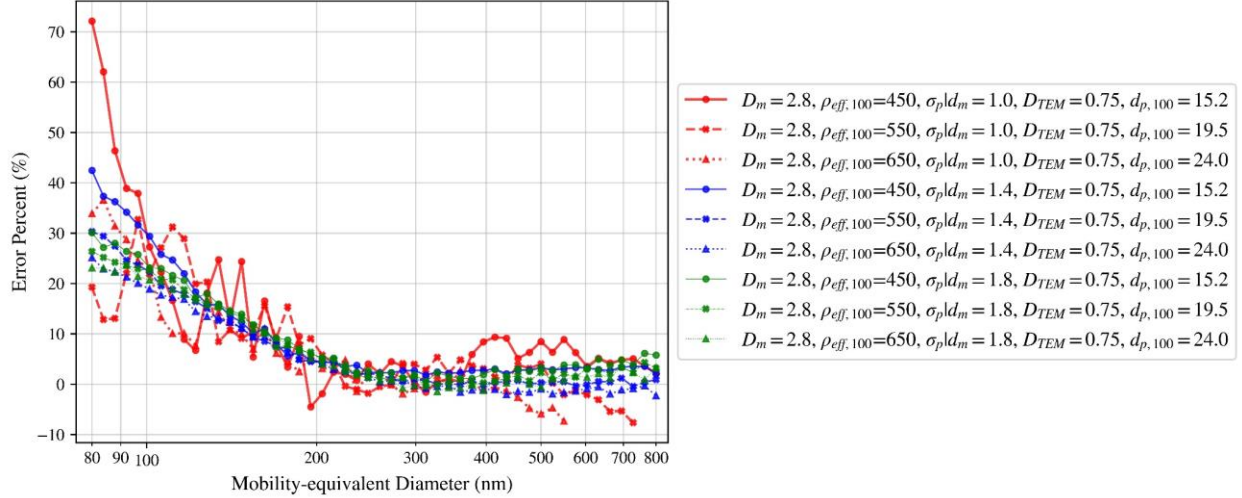


Figure 41

Percentage Error for TMatrix and RDG-FA Scattering Cross Section for $\rho_{eff,100} = 450 \text{ kg/m}^3$

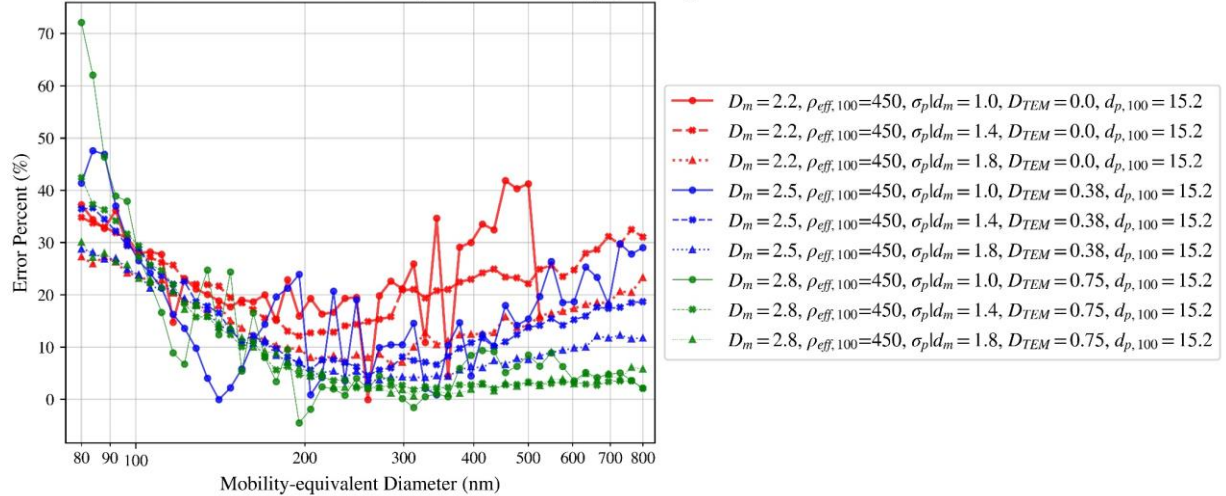


Figure 42

Percentage Error for TMATRIX and RDG-FA Scattering Cross Section for $\rho_{eff,100} = 550 \text{ kg/m}^3$

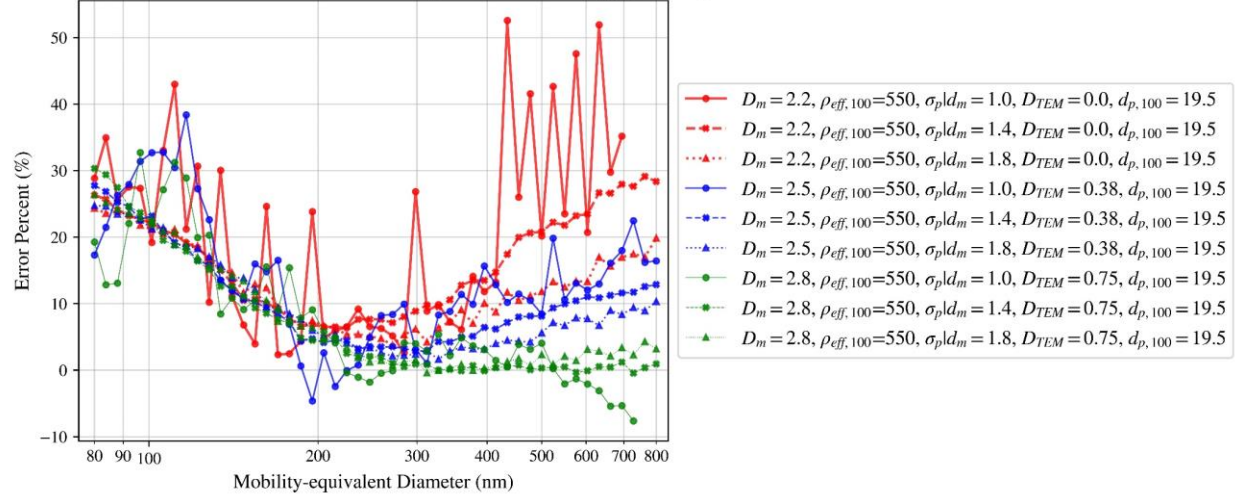


Figure 43

Percentage Error for TMATRIX and RDG-FA Scattering Cross Section for $\rho_{eff,100} = 650 \text{ kg/m}^3$

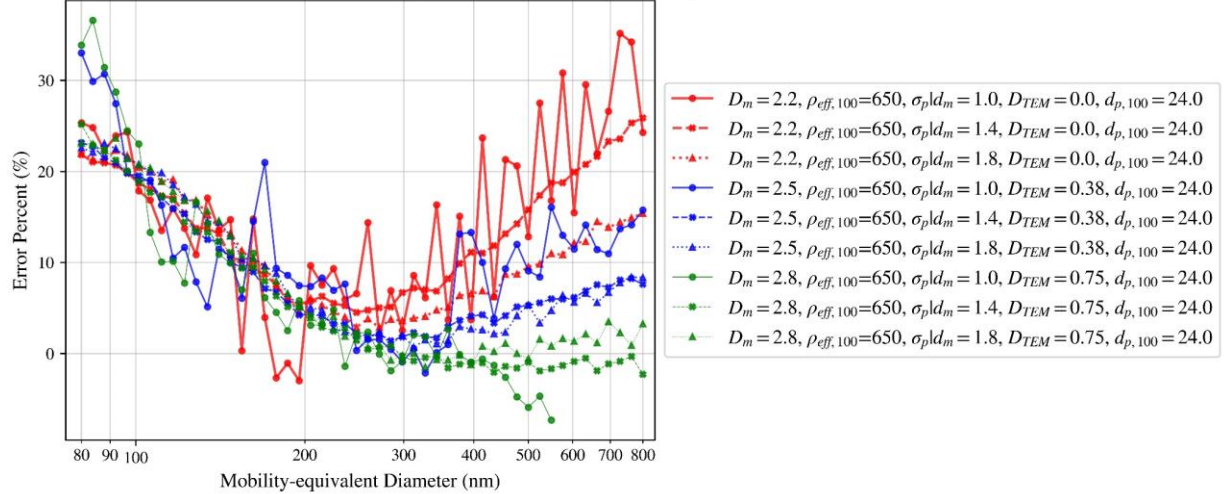


Figure 44

Percentage Error for TMatrix and RDG-FA Scattering Cross Section for $\sigma_p|d_m = 1.0$

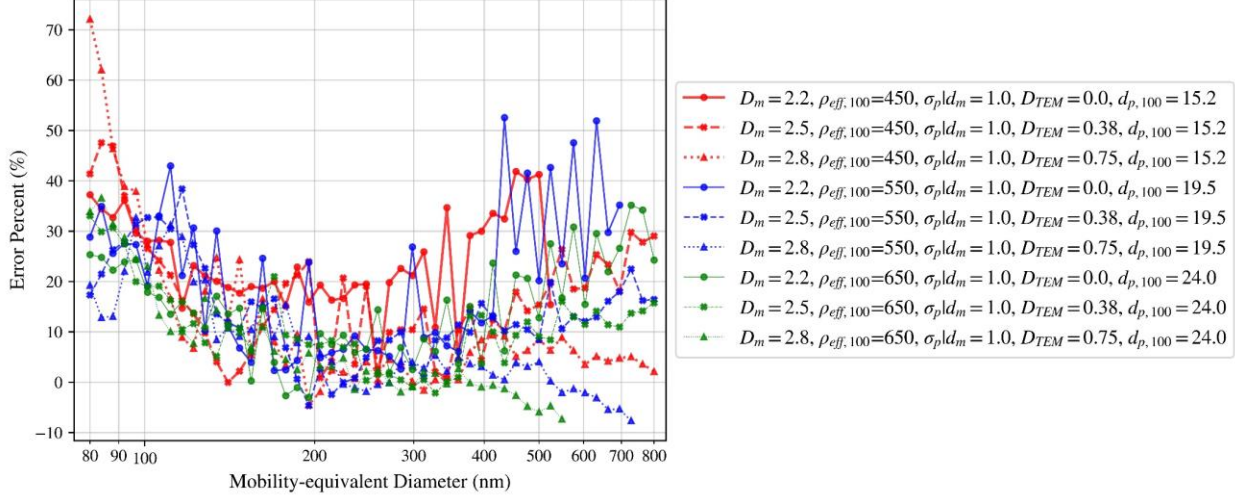


Figure 45

Percentage Error for TMatrix and RDG-FA Scattering Cross Section for $\sigma_p|d_m = 1.4$

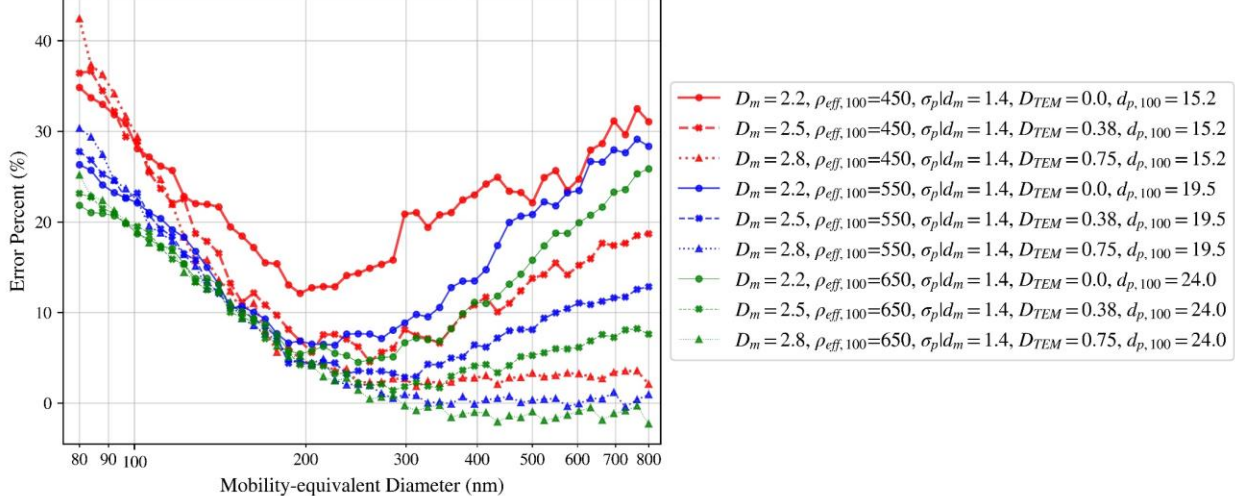


Figure 46

Percentage Error for TMatrix and RDG-FA Scattering Cross Section for $\sigma_p|d_m = 1.8$

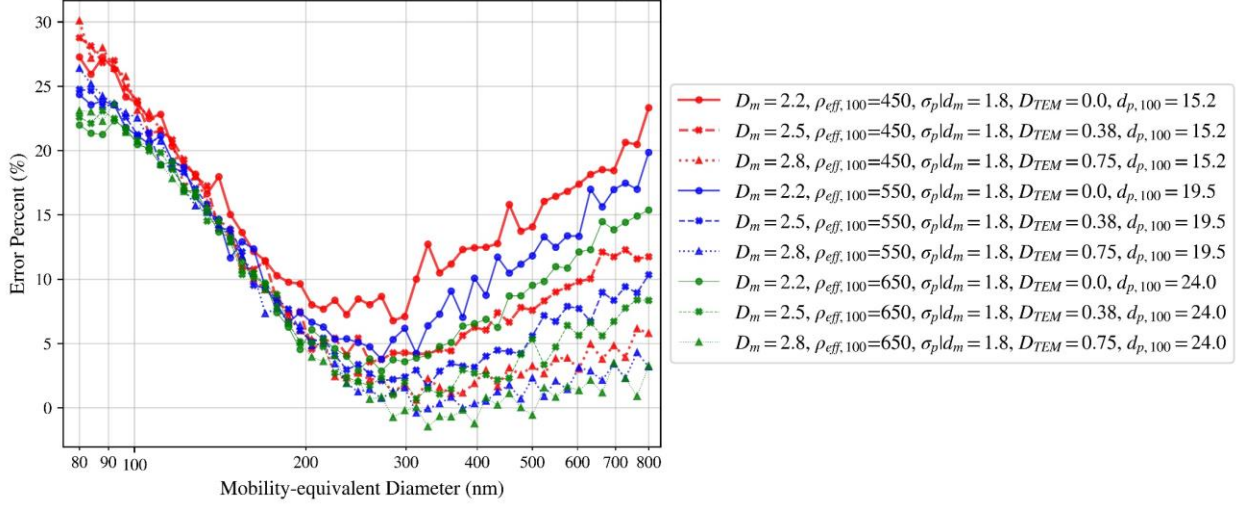


Figure 47

12. T-matrix and RDG-FA absorption cross-section ratio

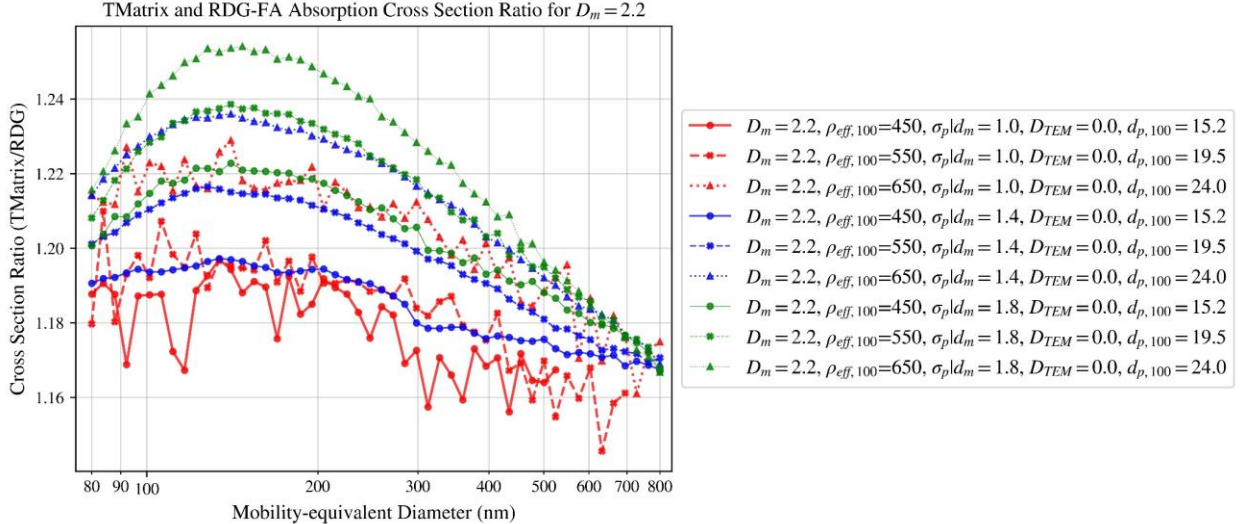


Figure 48

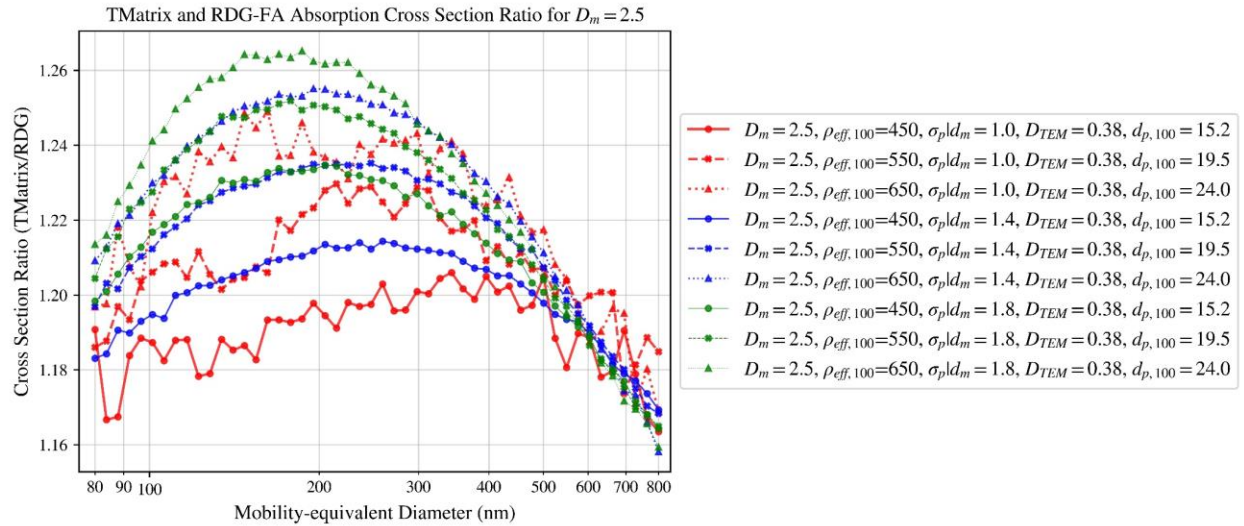


Figure 49

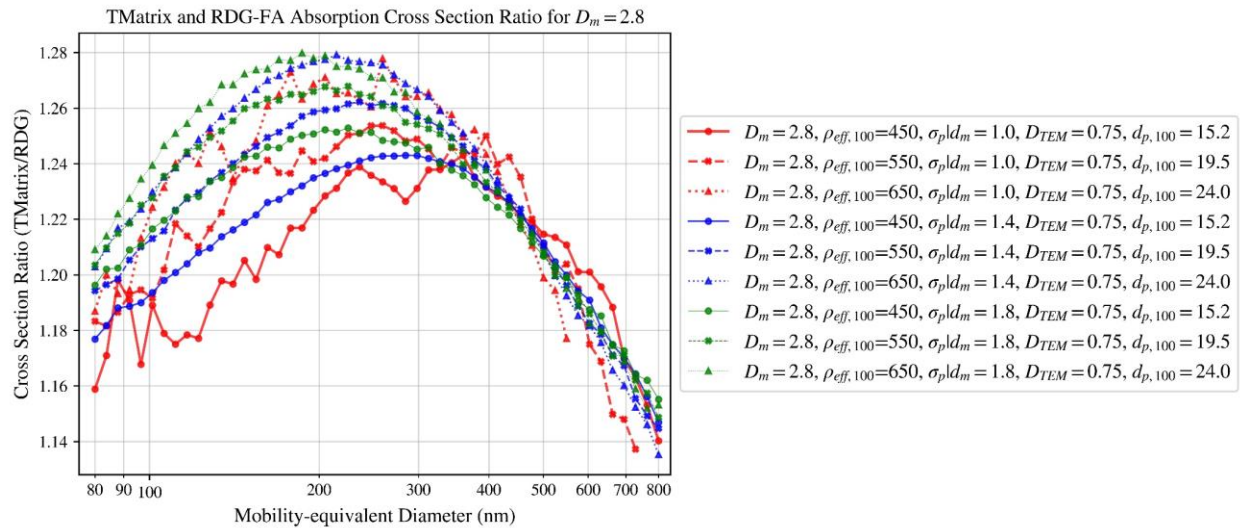


Figure 50

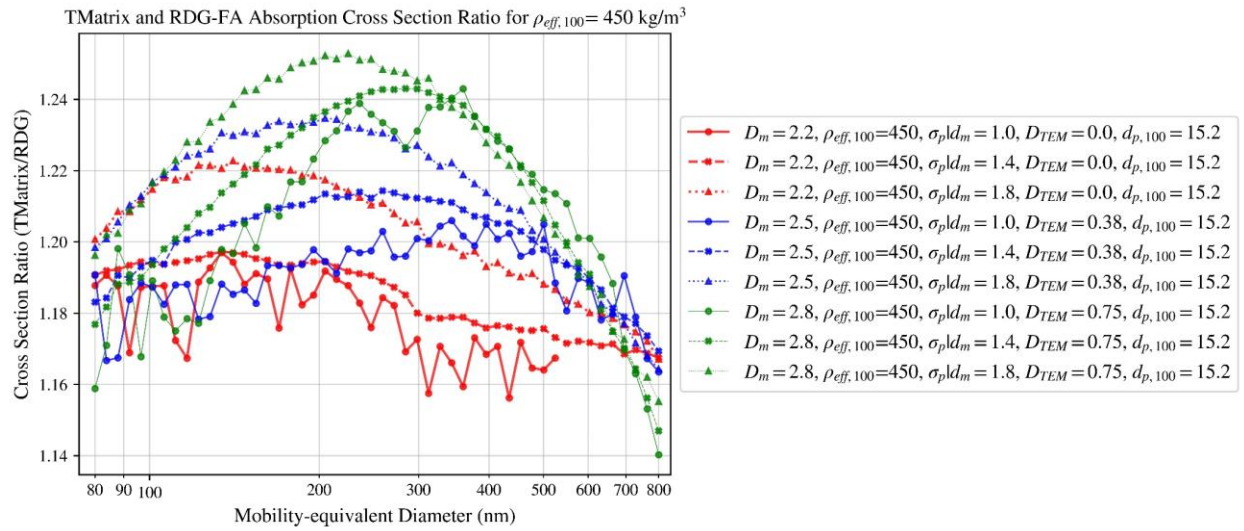


Figure 51

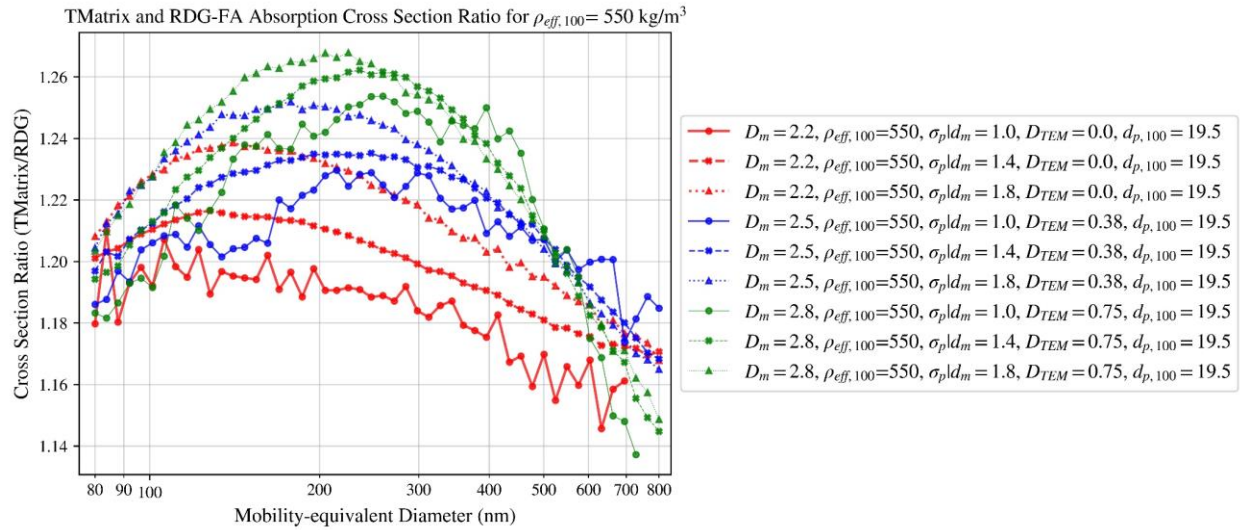


Figure 52

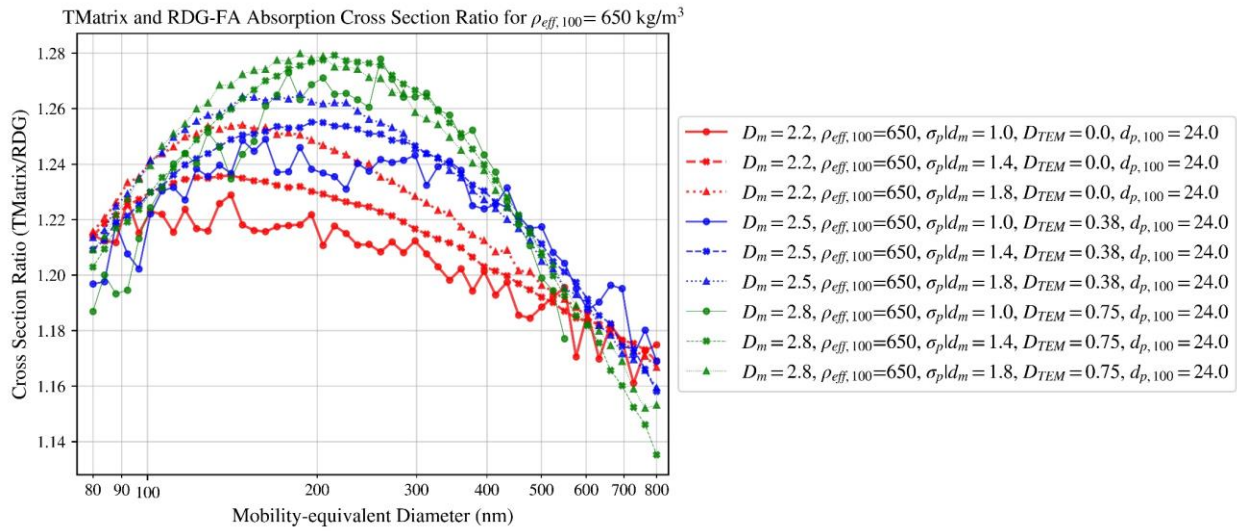


Figure 53

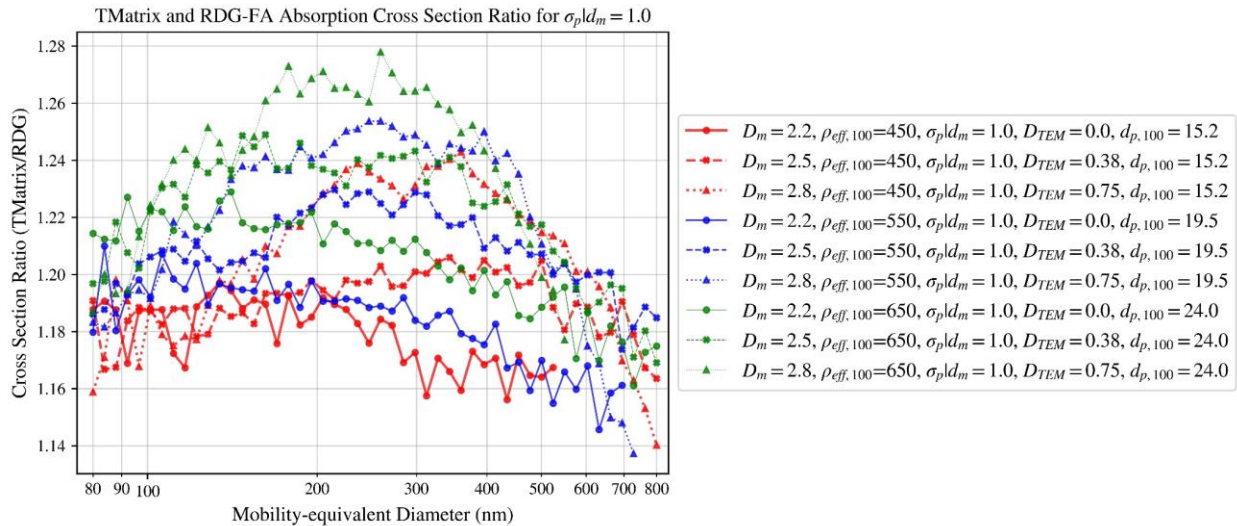


Figure 54

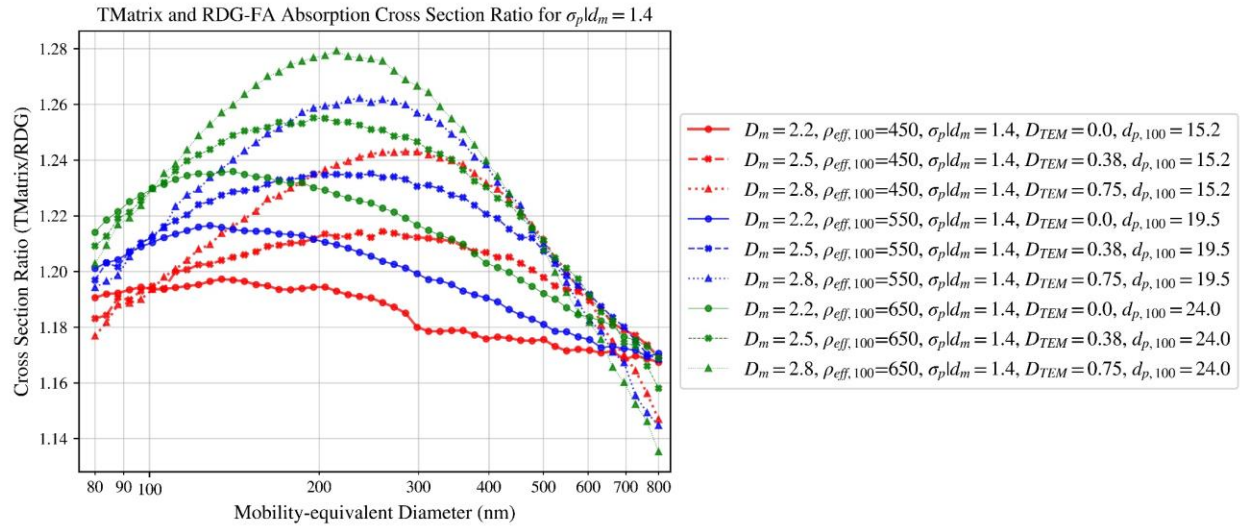


Figure 55

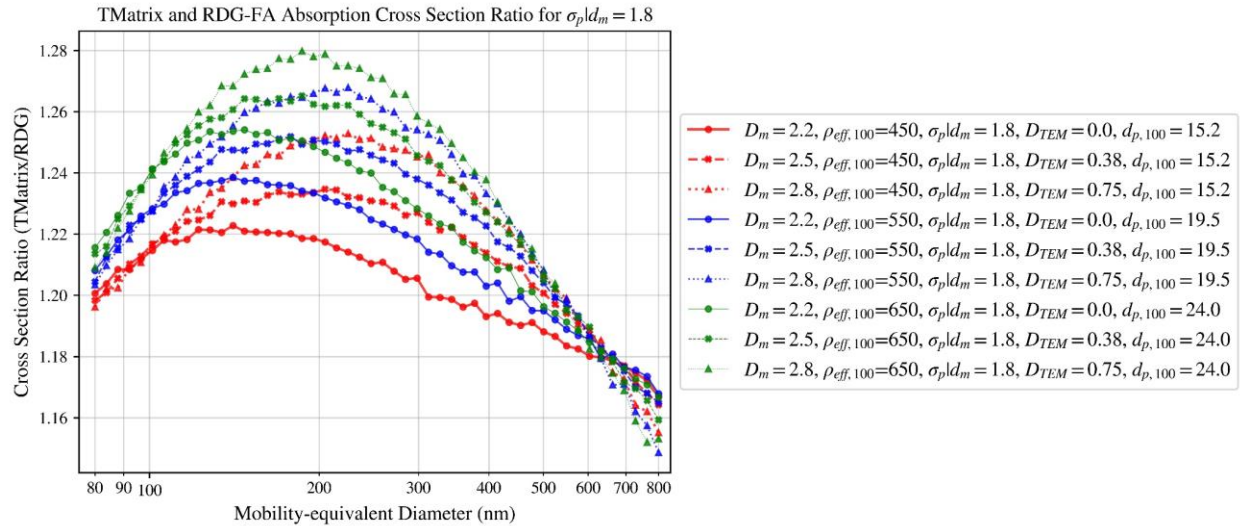


Figure 56

13. T-matrix and RDG-FA scattering cross-section ratio

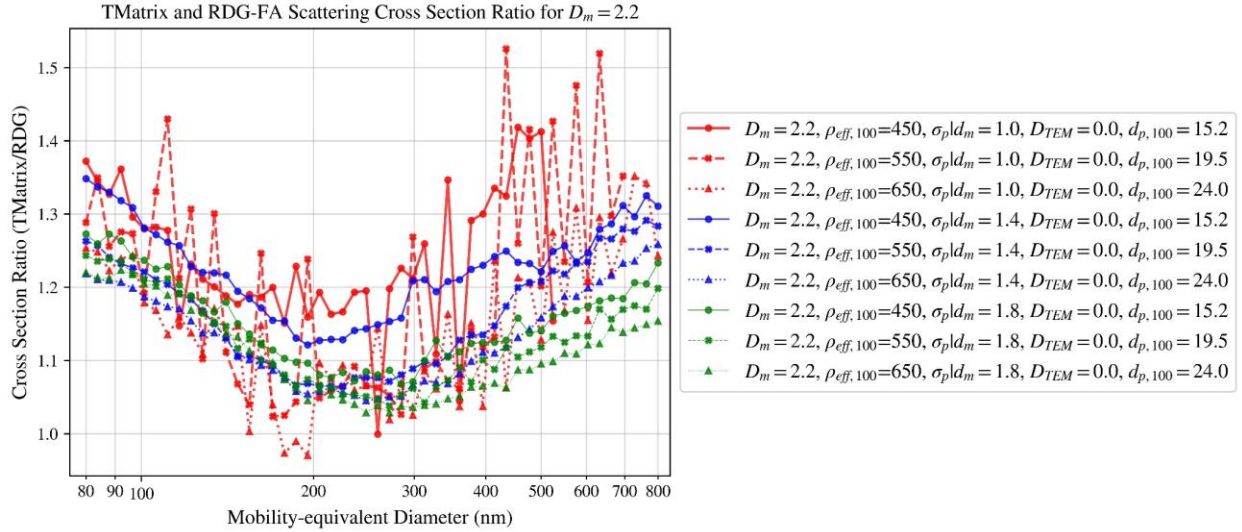


Figure 57

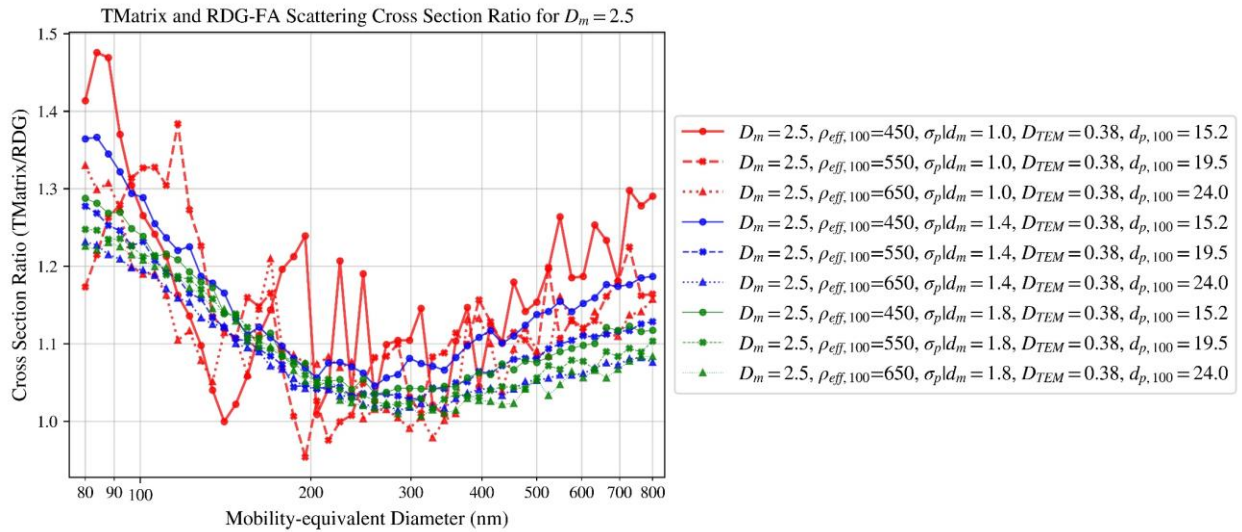


Figure 58

TMatrix and RDG-FA Scattering Cross Section Ratio for $D_m = 2.8$

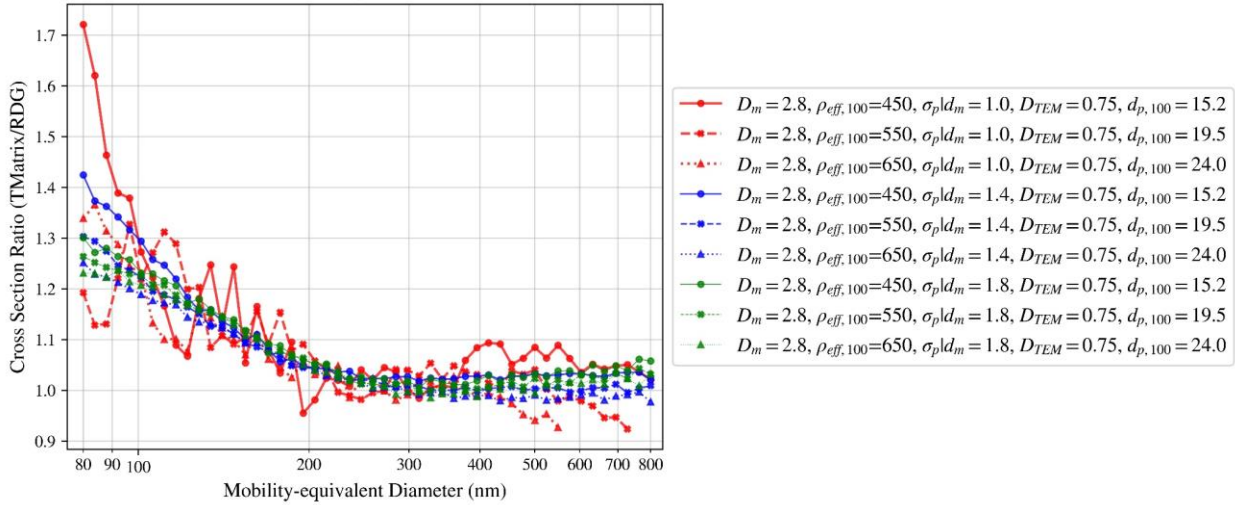


Figure 59

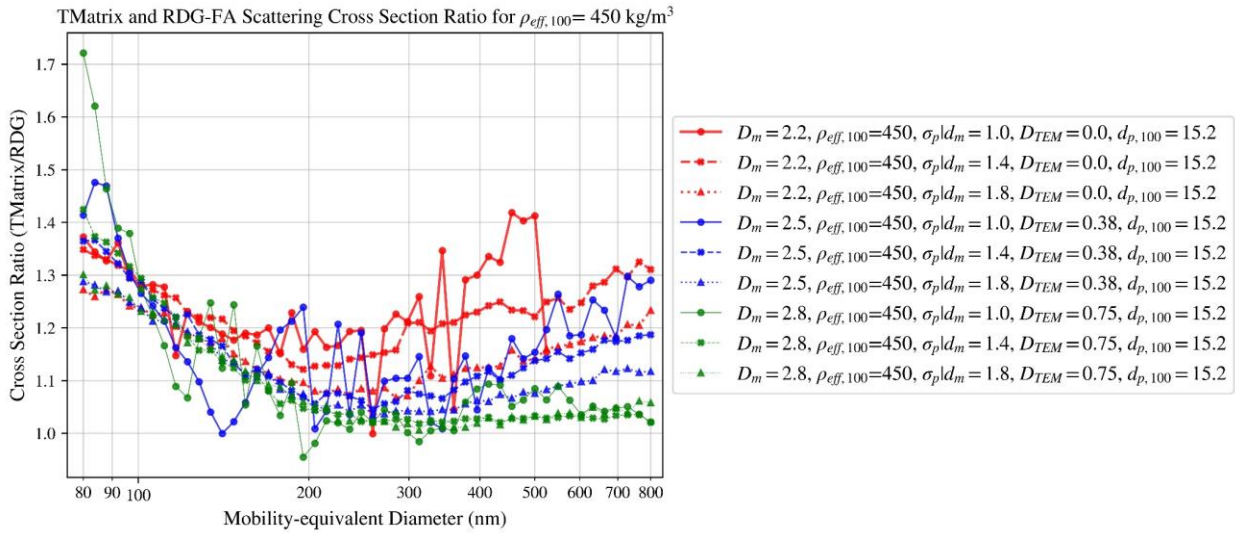


Figure 60

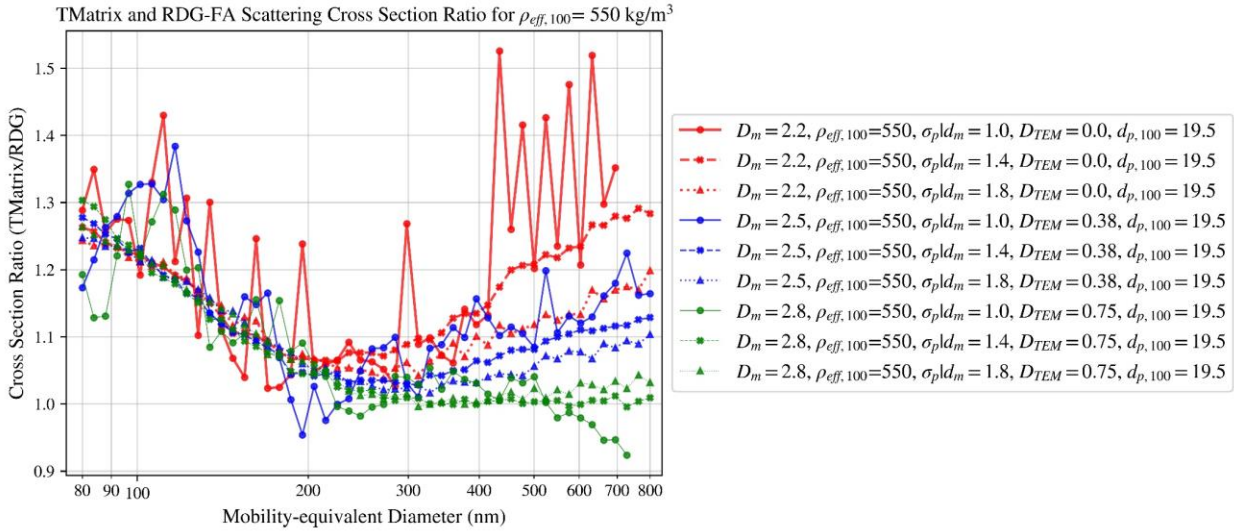


Figure 61

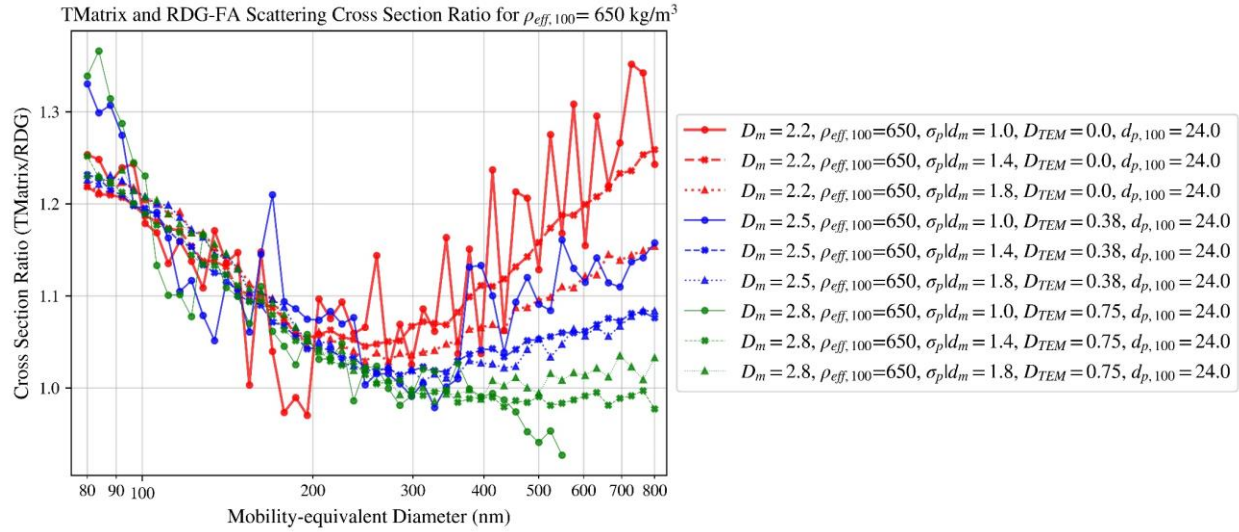


Figure 62

TMatrix and RDG-FA Scattering Cross Section Ratio for $\sigma_p|d_m = 1.0$

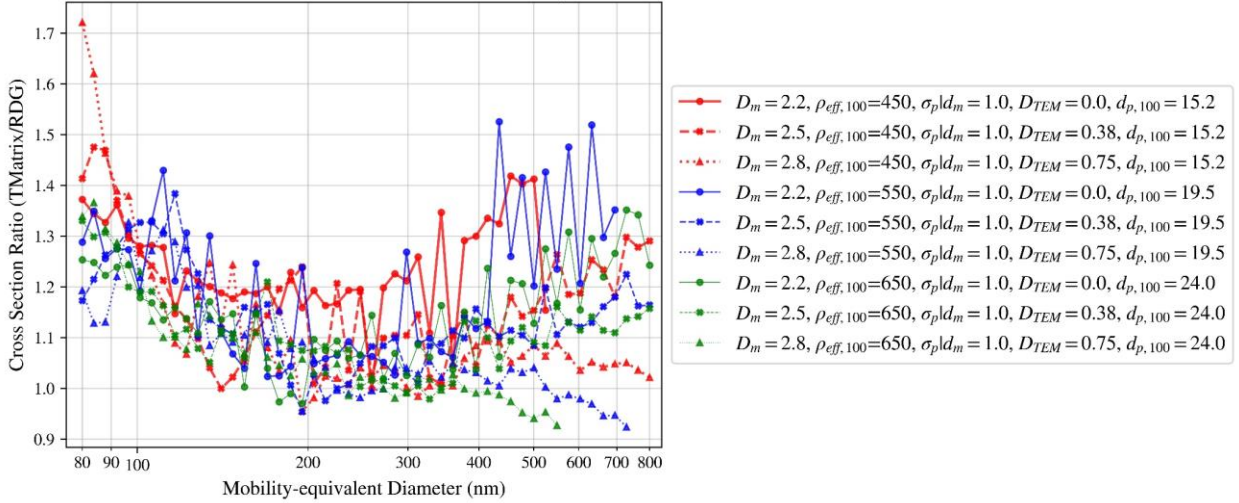


Figure 63

TMatrix and RDG-FA Scattering Cross Section Ratio for $\sigma_p|d_m = 1.4$

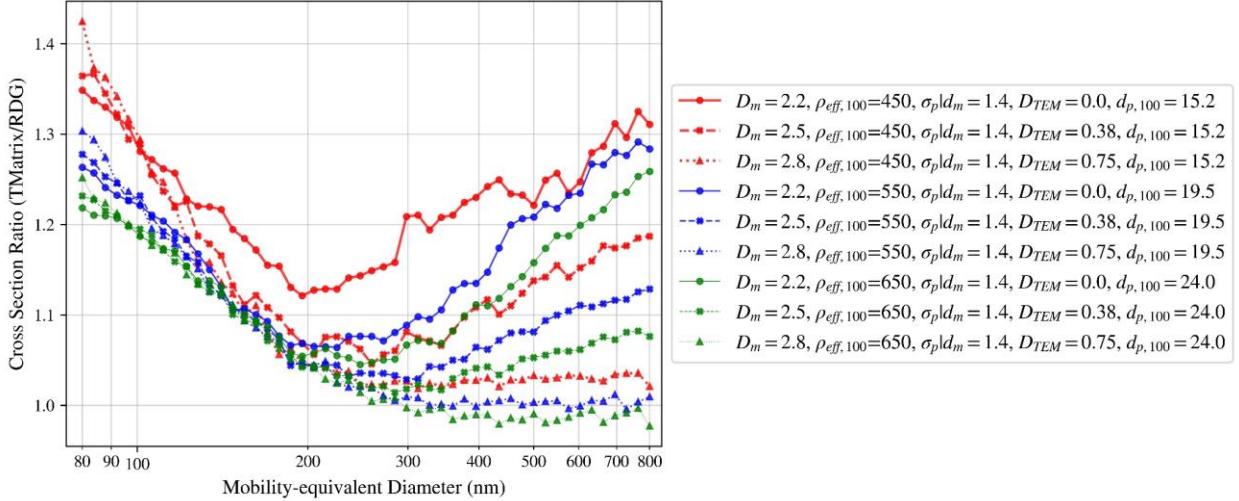


Figure 64

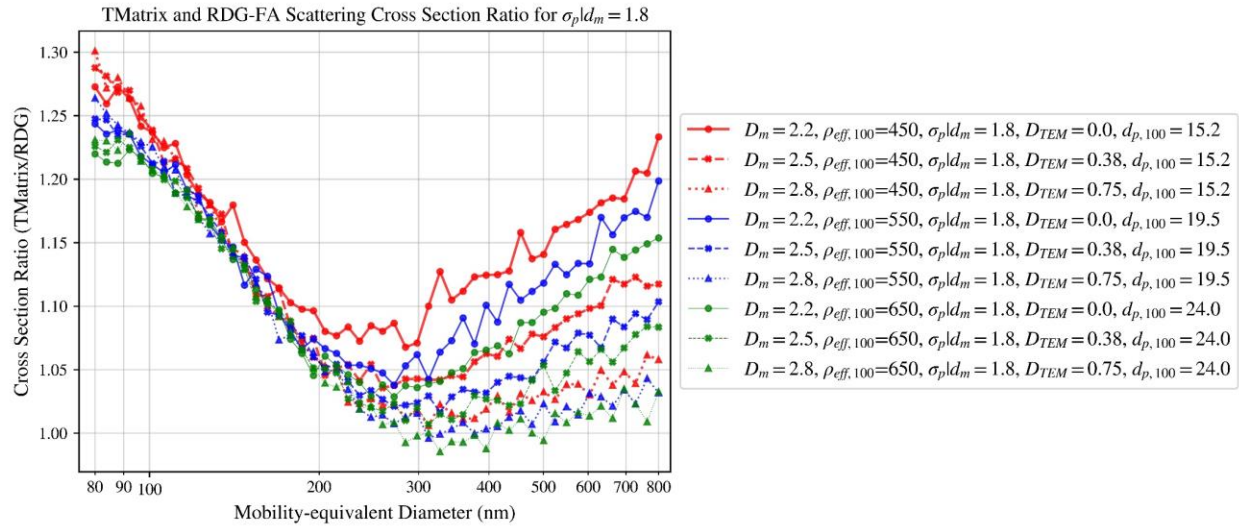


Figure 65

14. MAC for RDG-FA

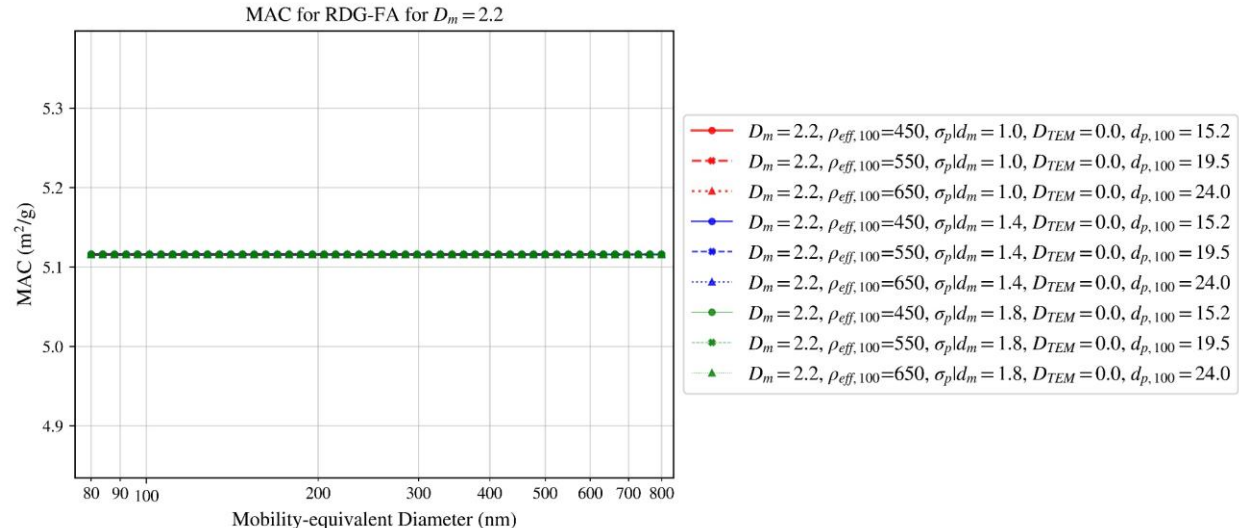


Figure 66

15. MSC for RDG-FA

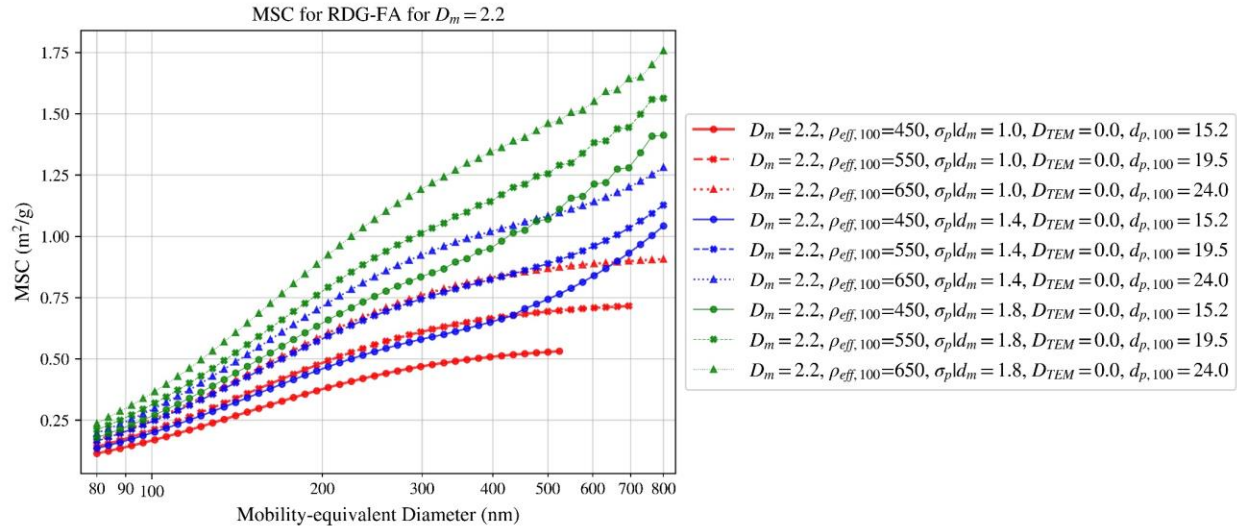


Figure 67

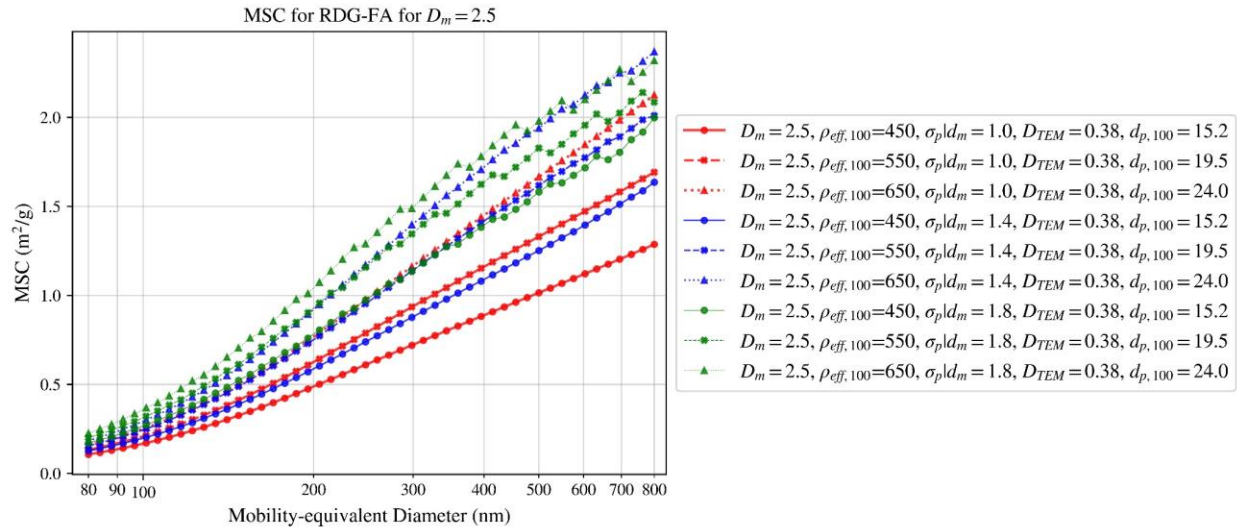


Figure 68

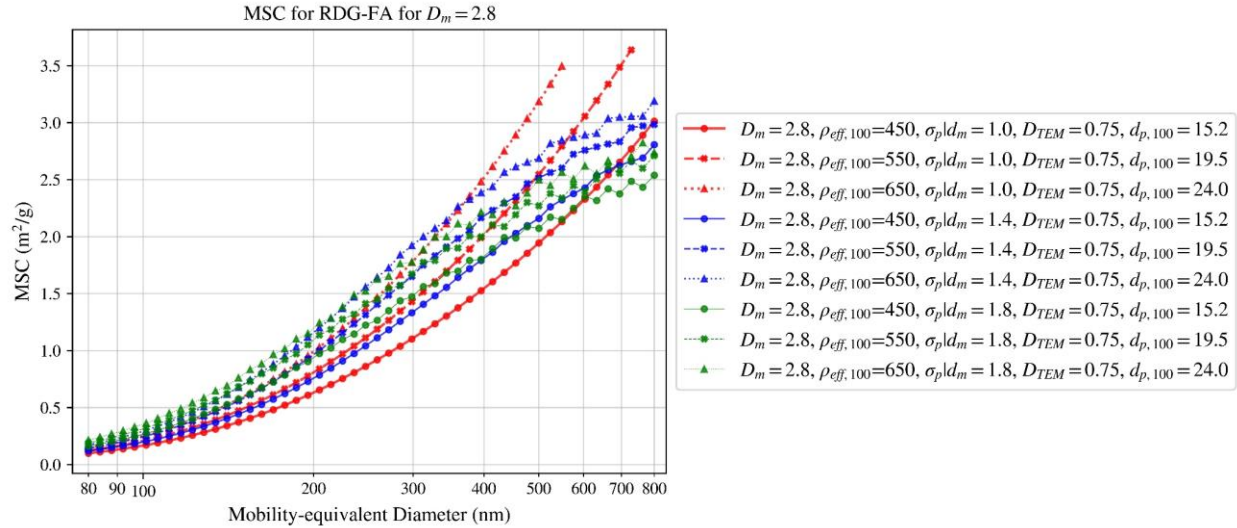


Figure 69

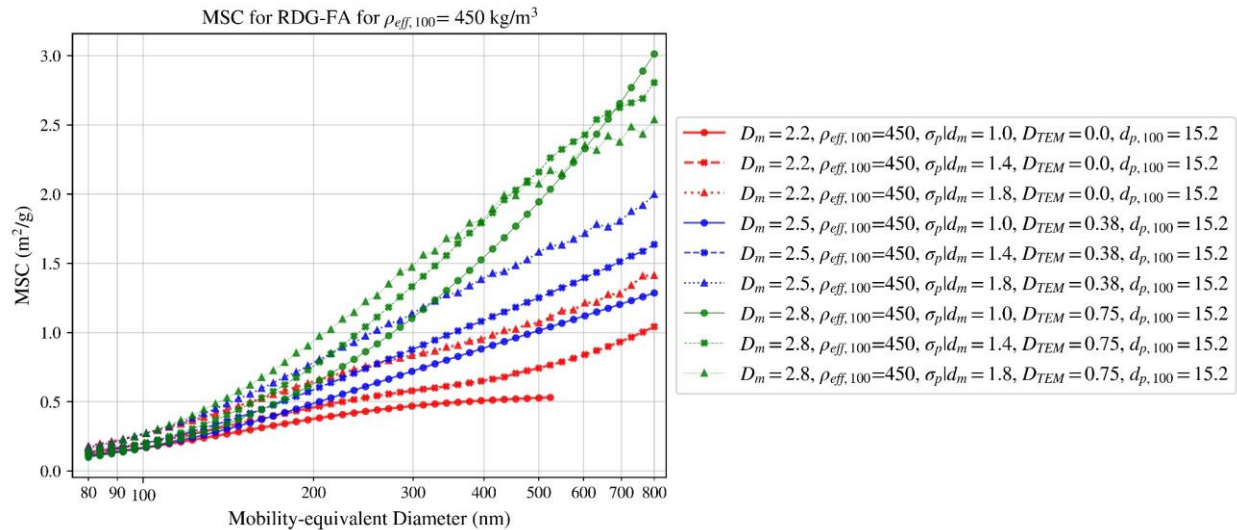


Figure 70

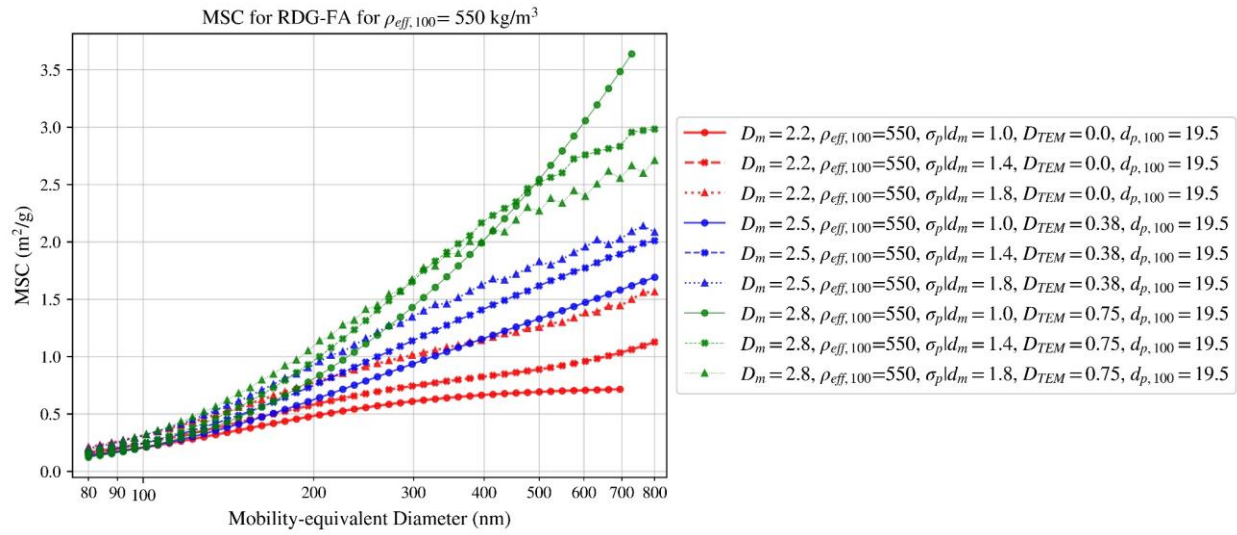


Figure 71

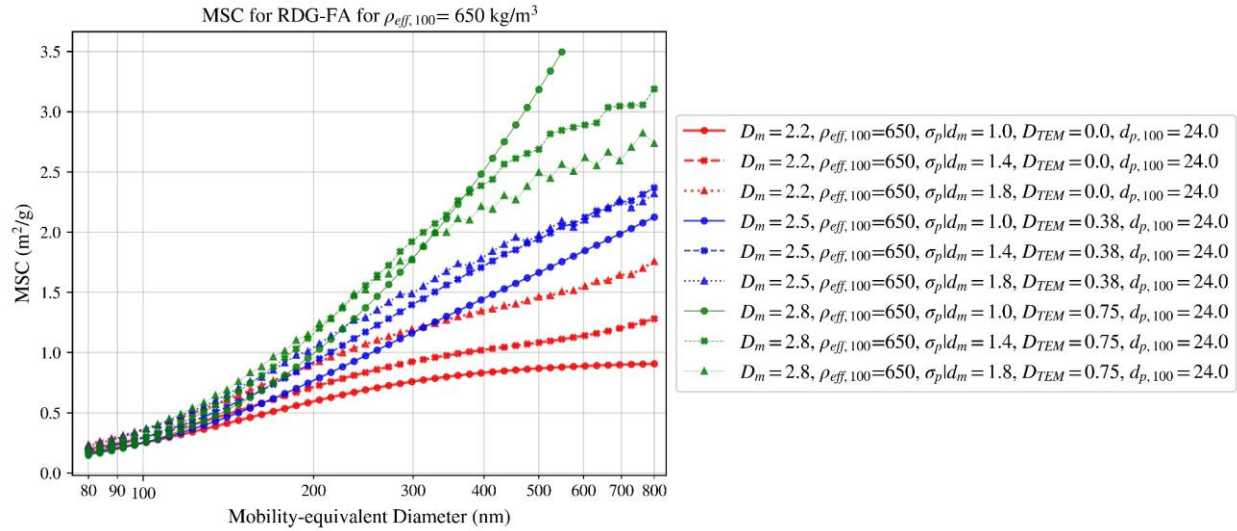


Figure 72

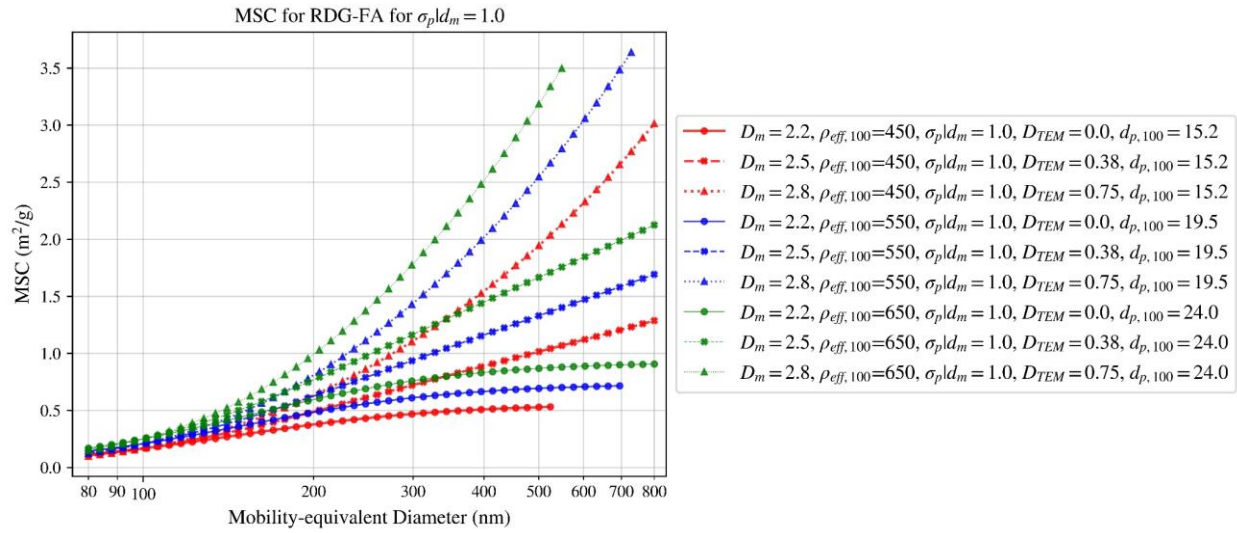


Figure 73

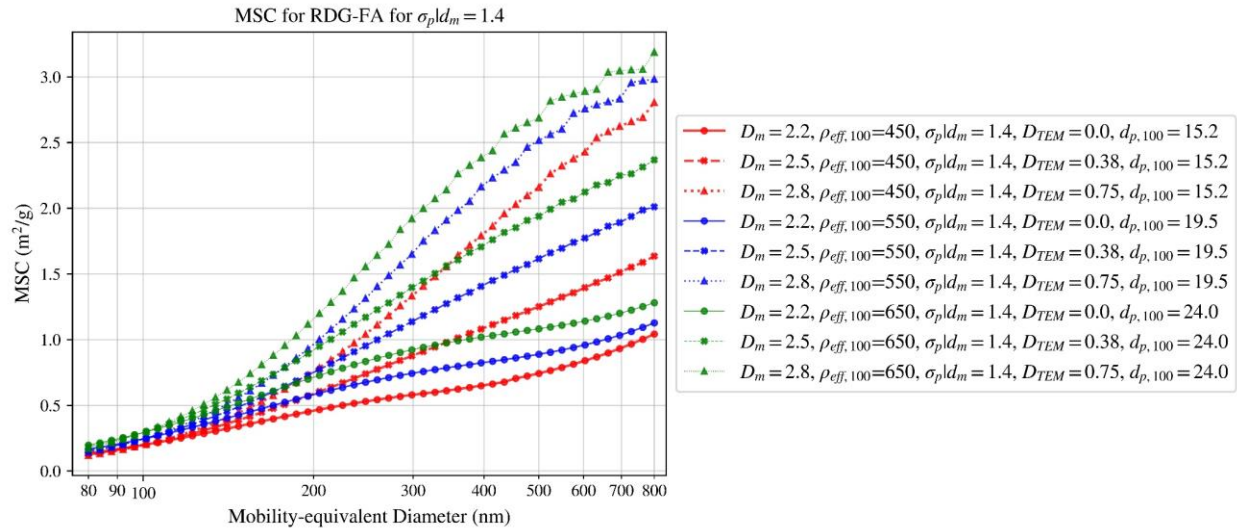


Figure 74

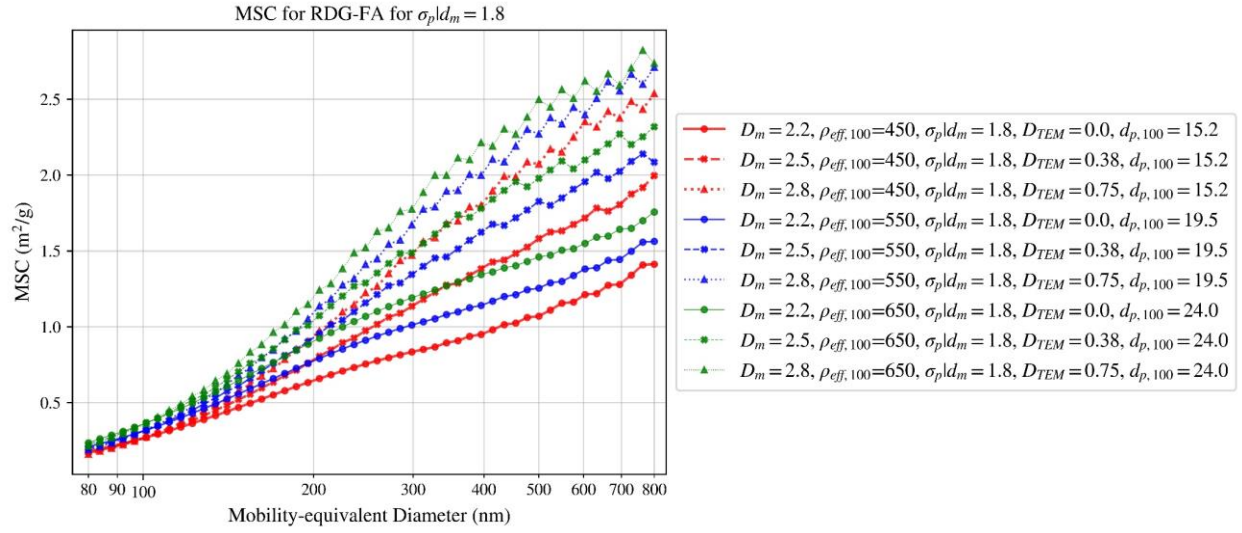


Figure 75

16. MAC for T-matrix

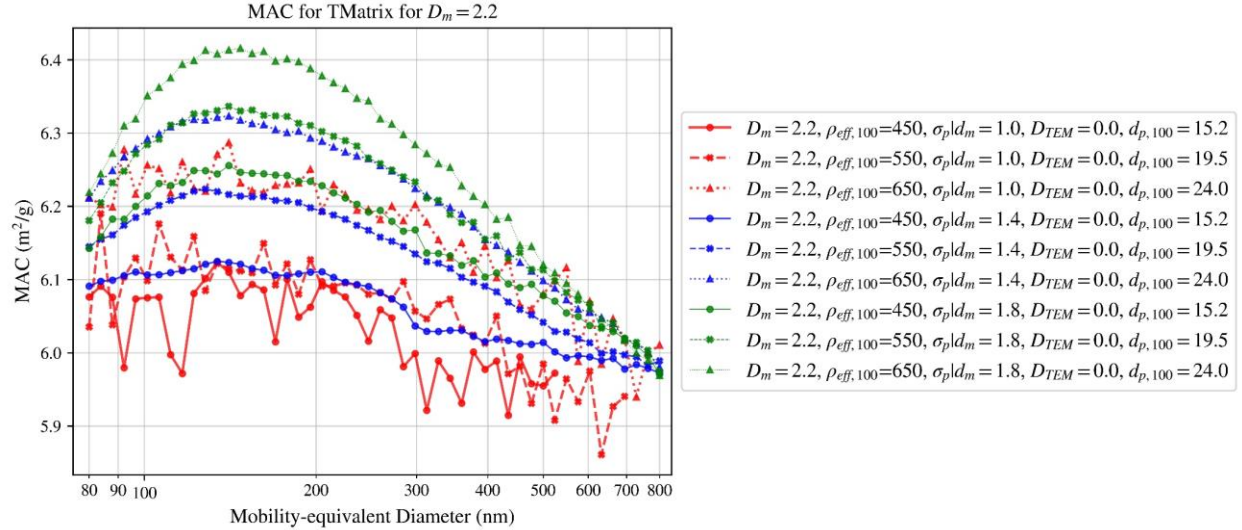


Figure 76

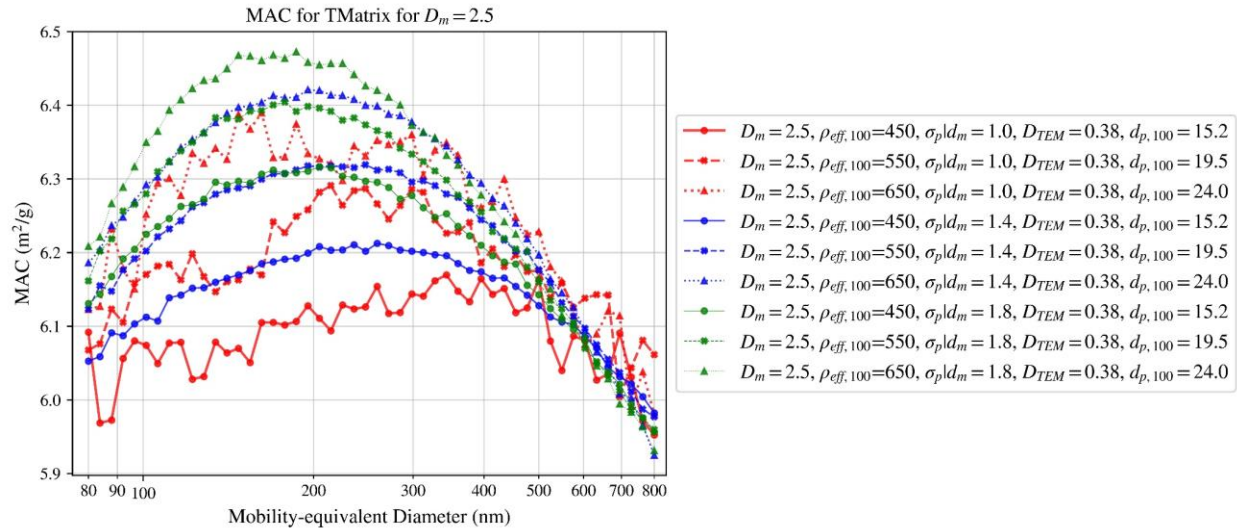


Figure 77

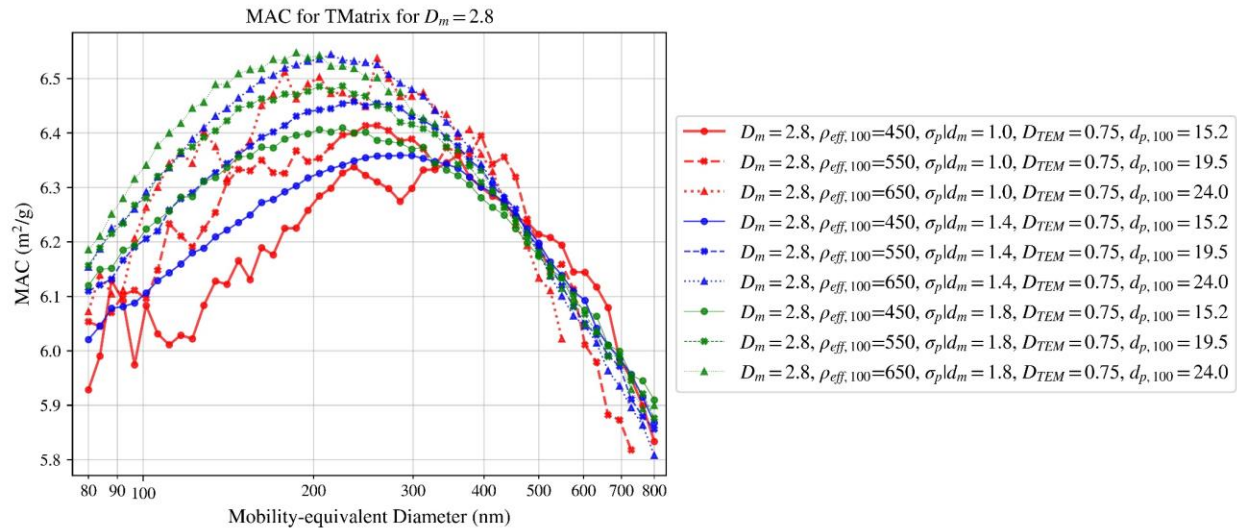


Figure 78

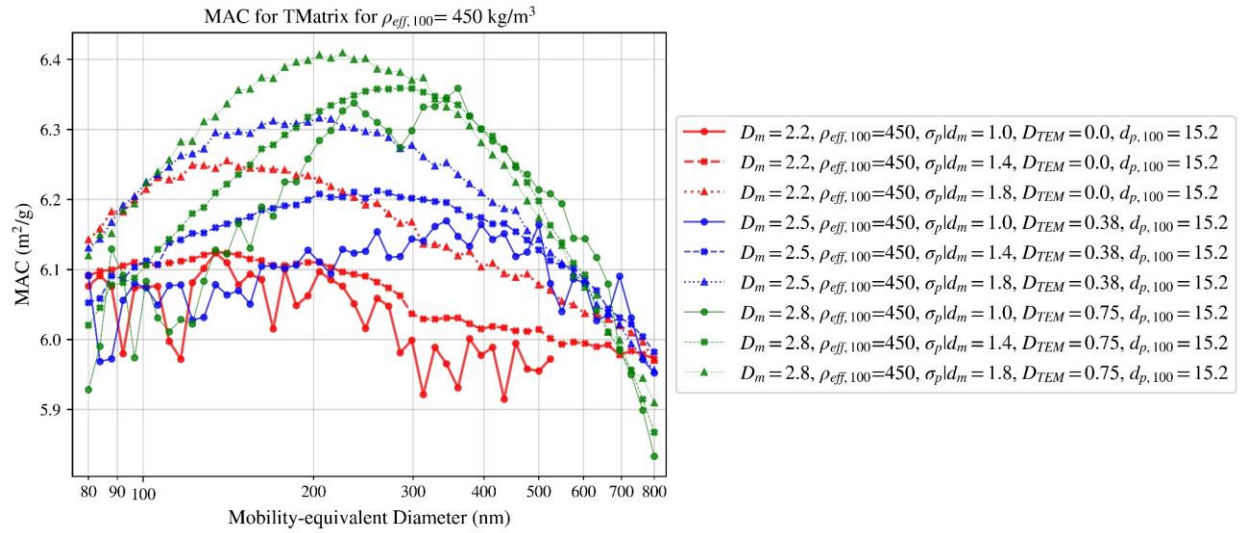


Figure 79

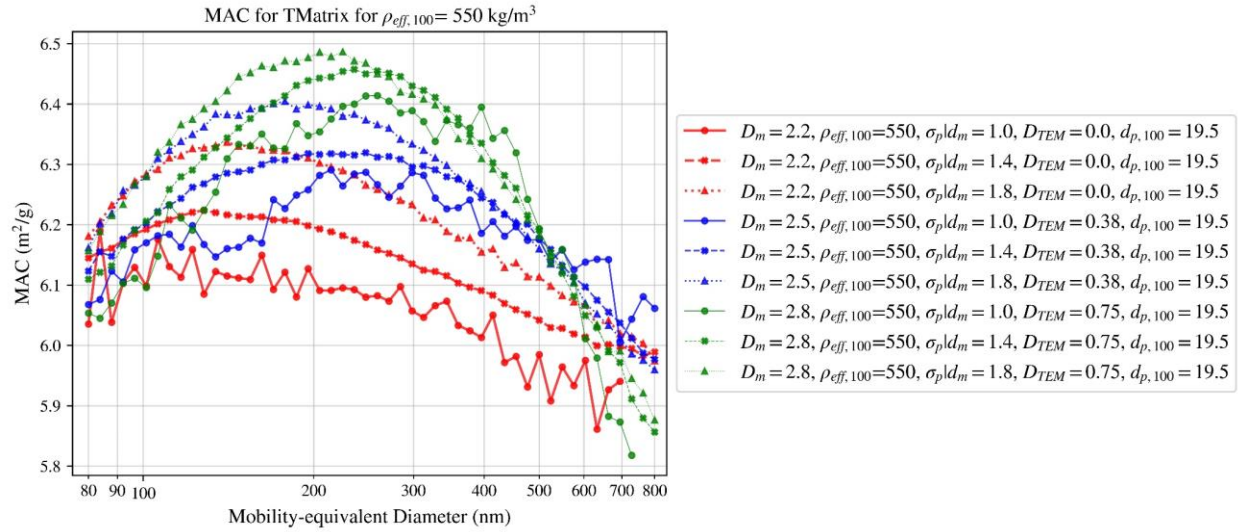


Figure 80

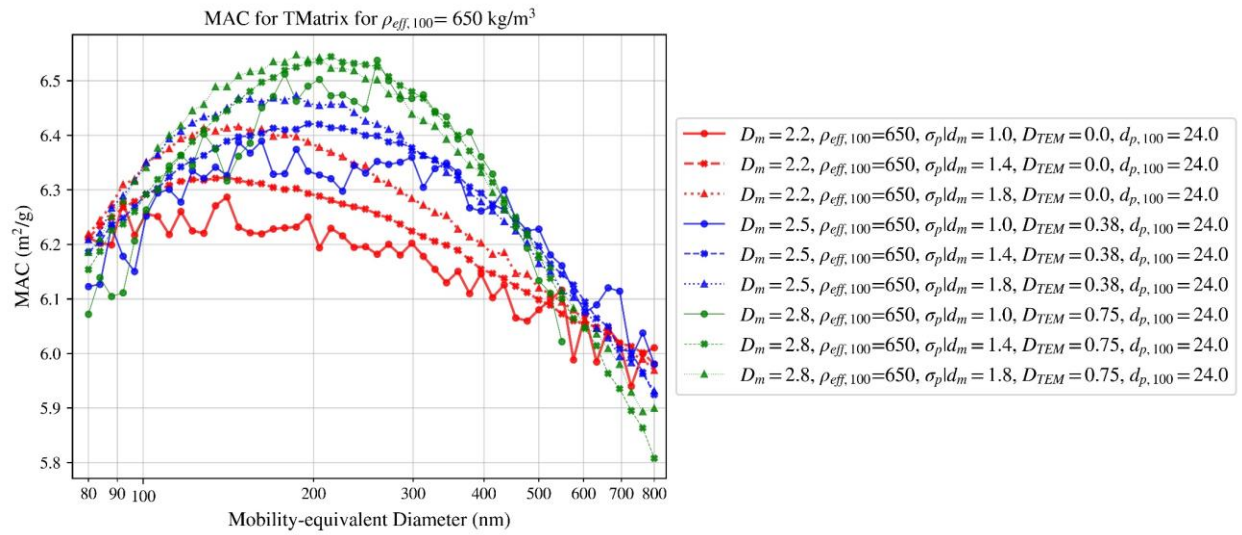


Figure 81

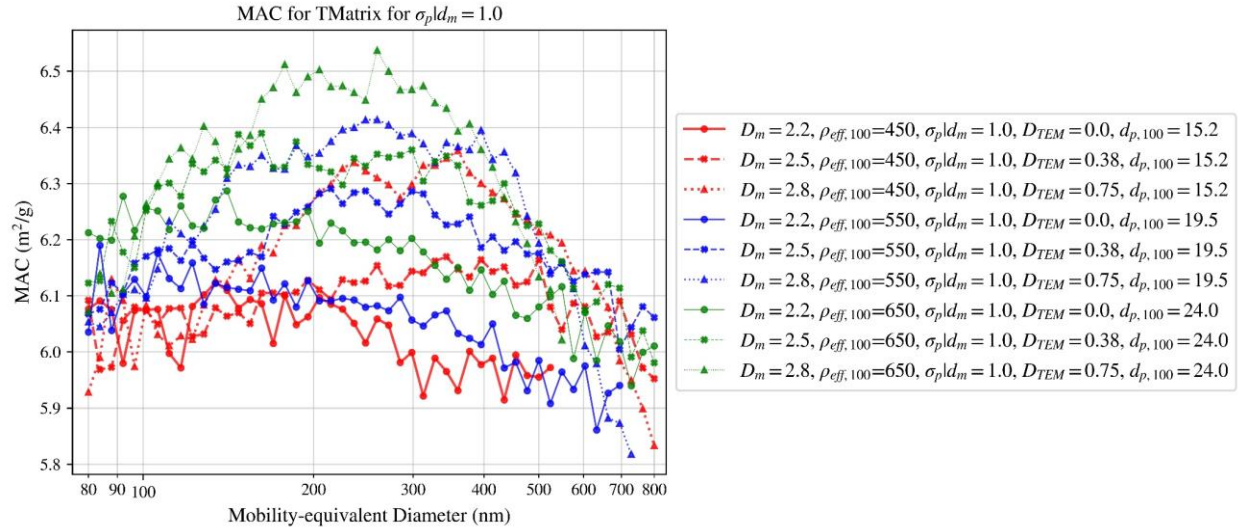


Figure 82

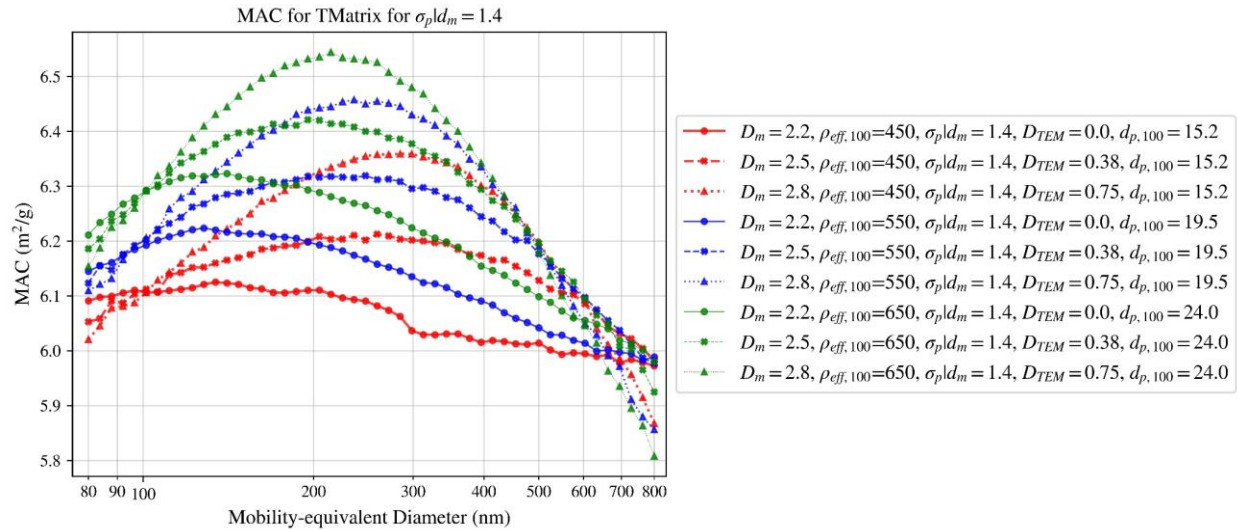


Figure 83

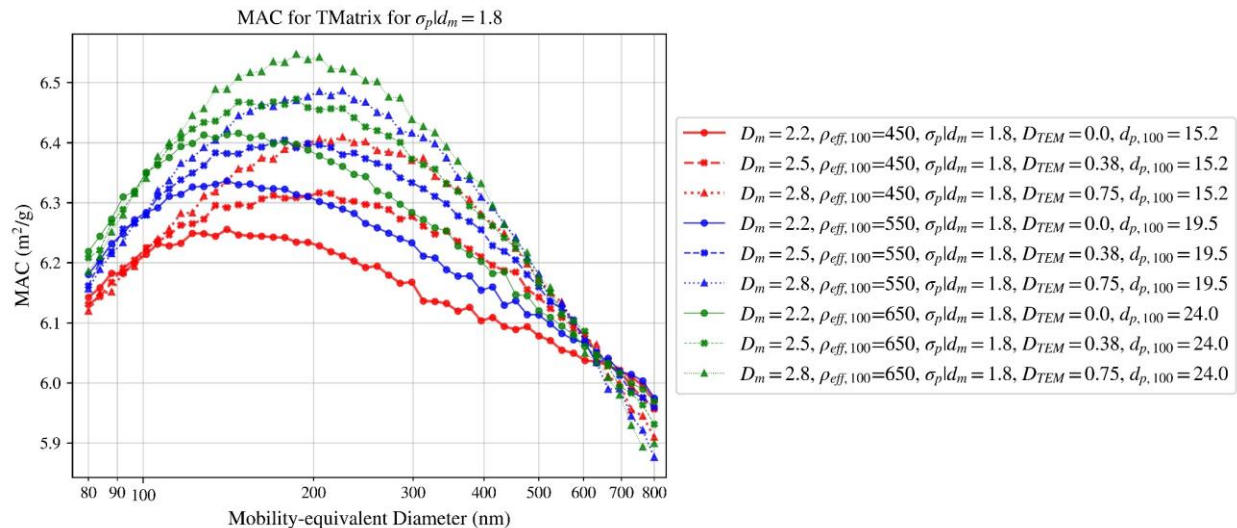


Figure 84

17. MSC for T-matrix

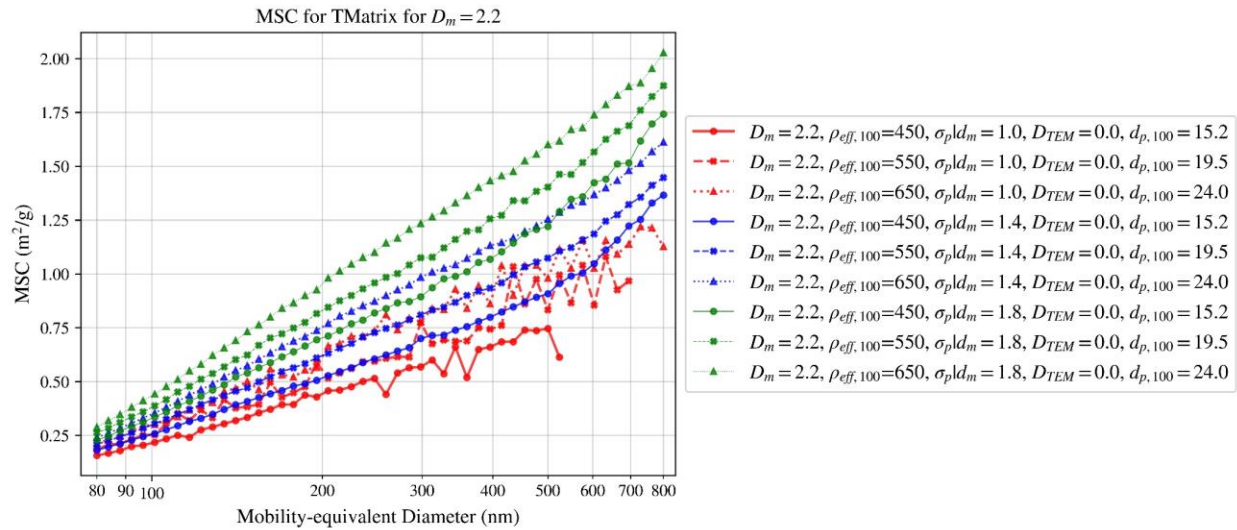


Figure 85

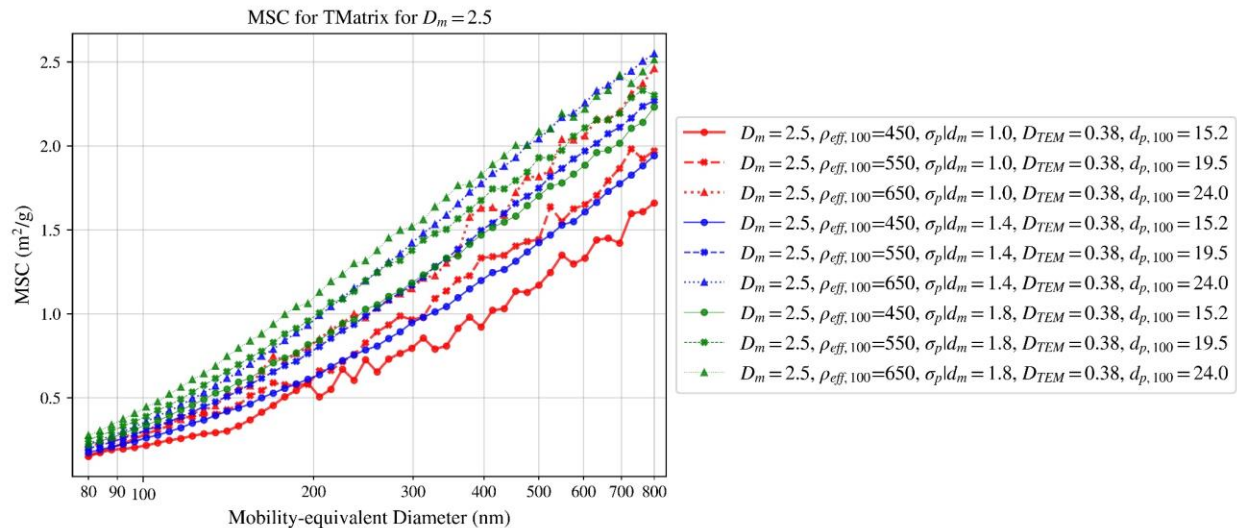


Figure 86

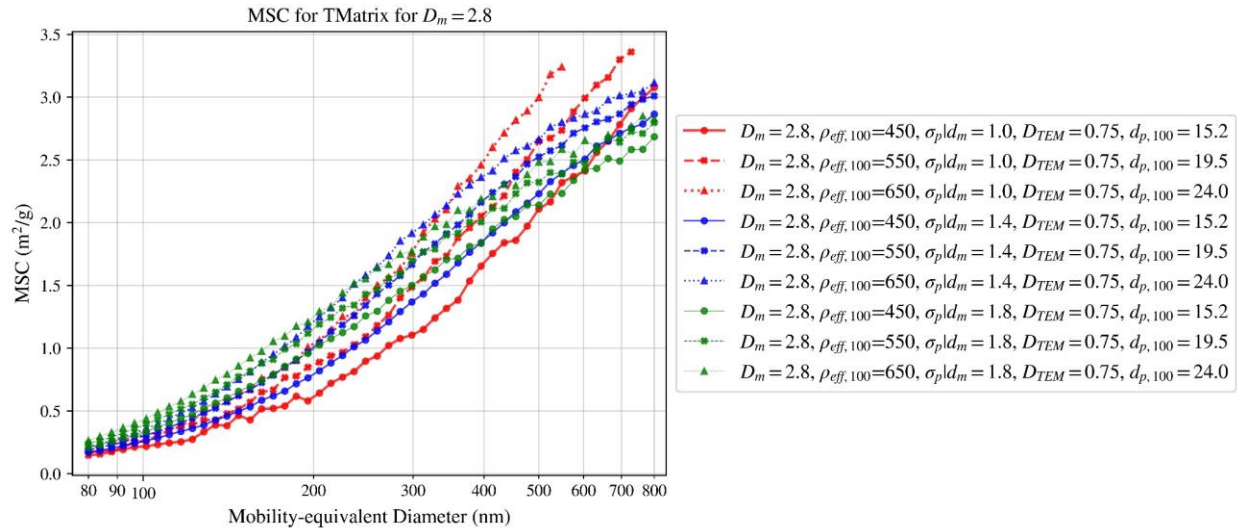


Figure 87

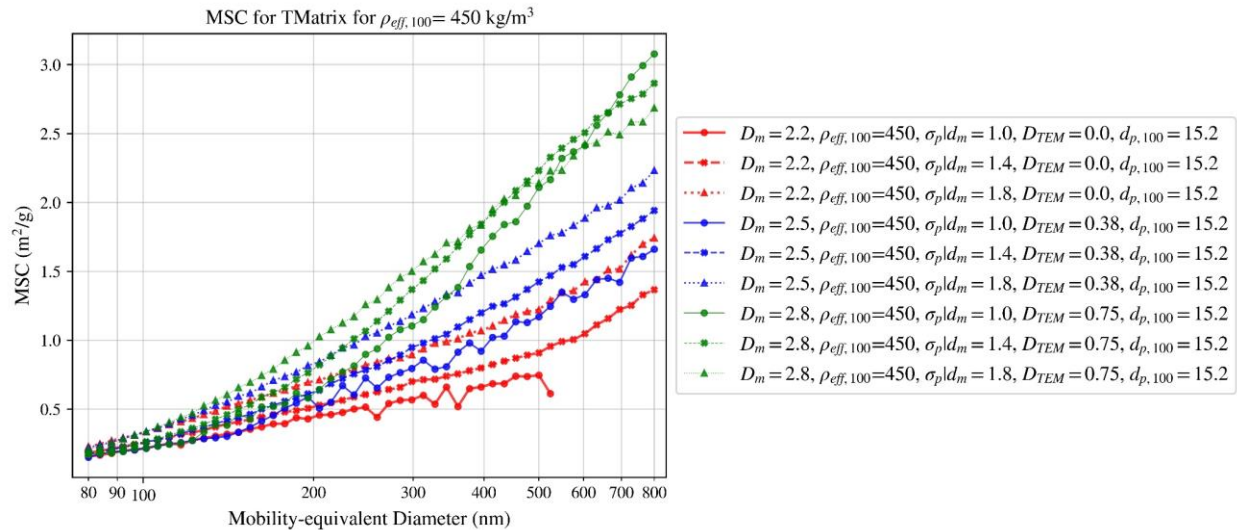


Figure 88

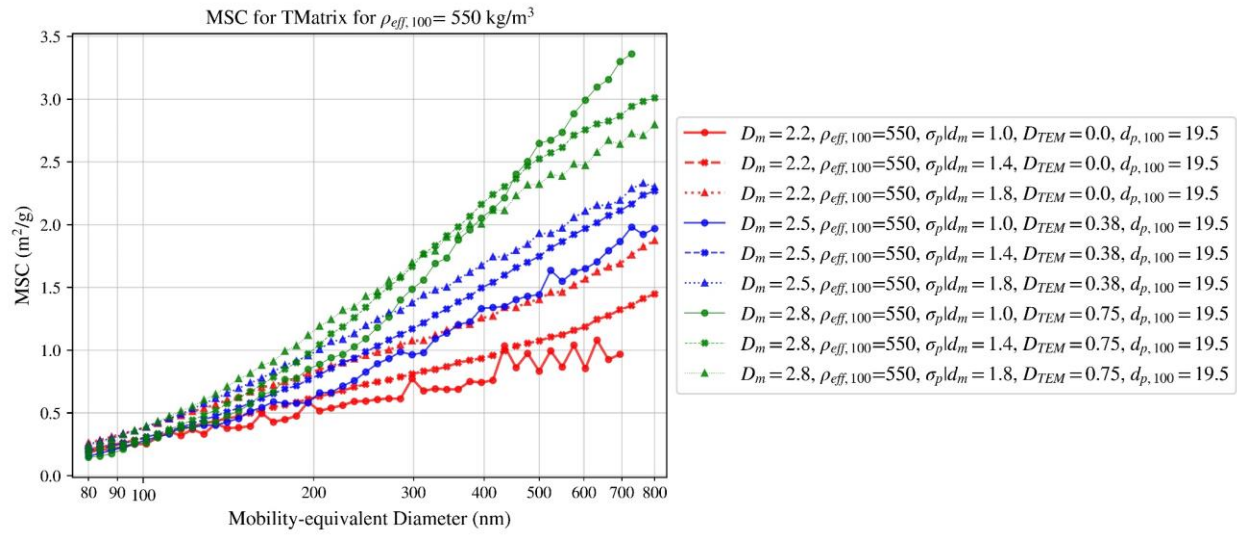


Figure 89

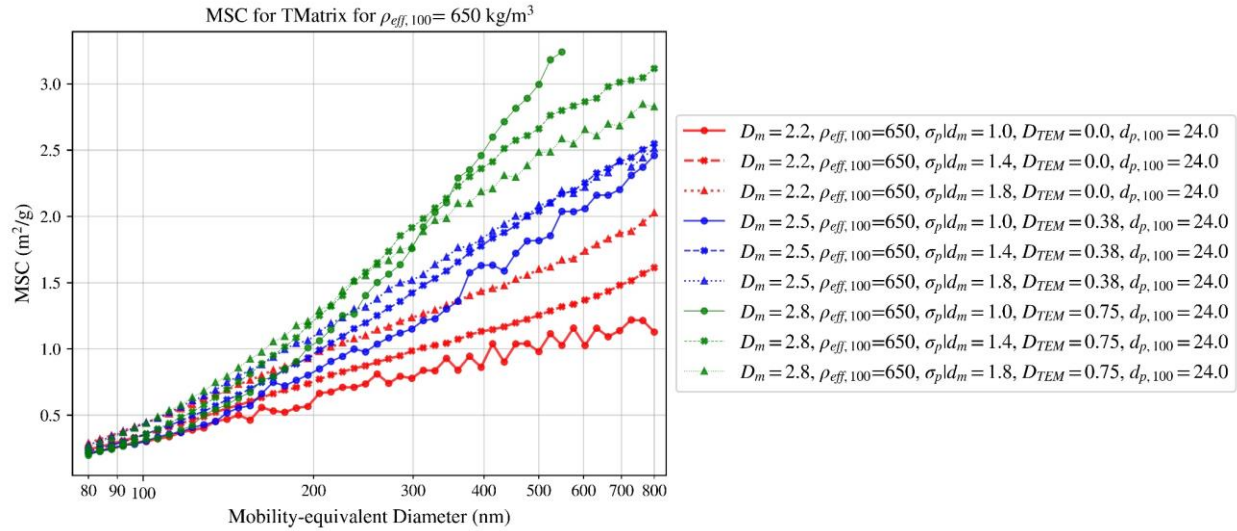


Figure 90

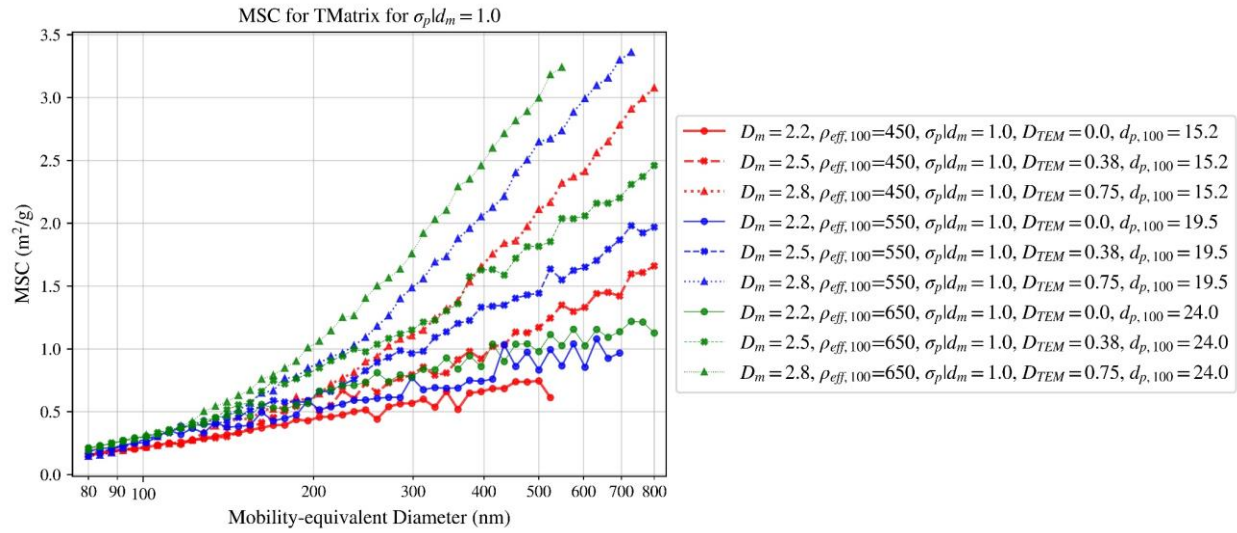


Figure 91

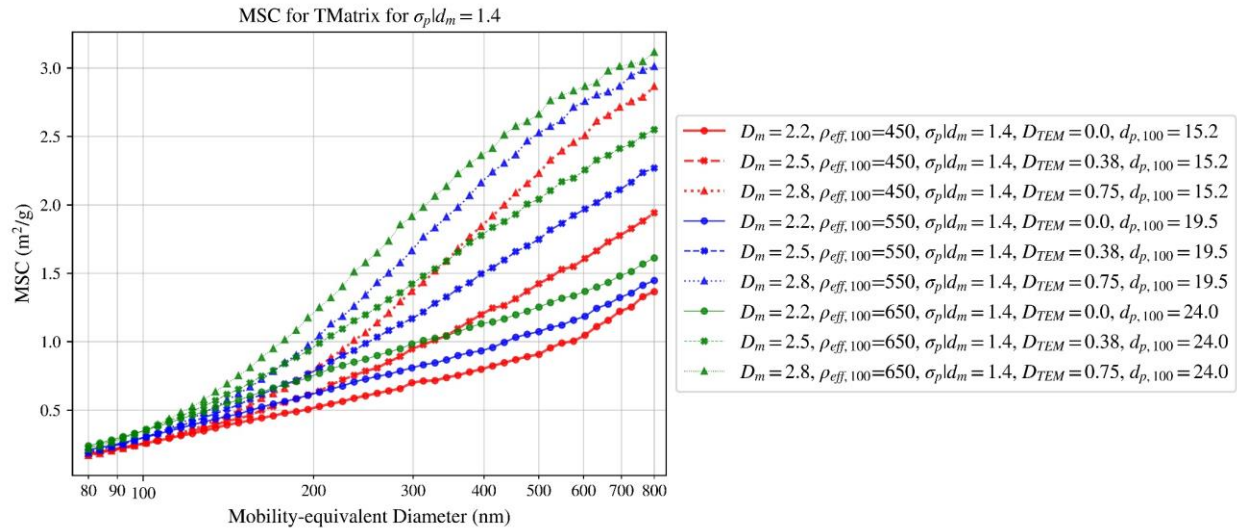


Figure 92

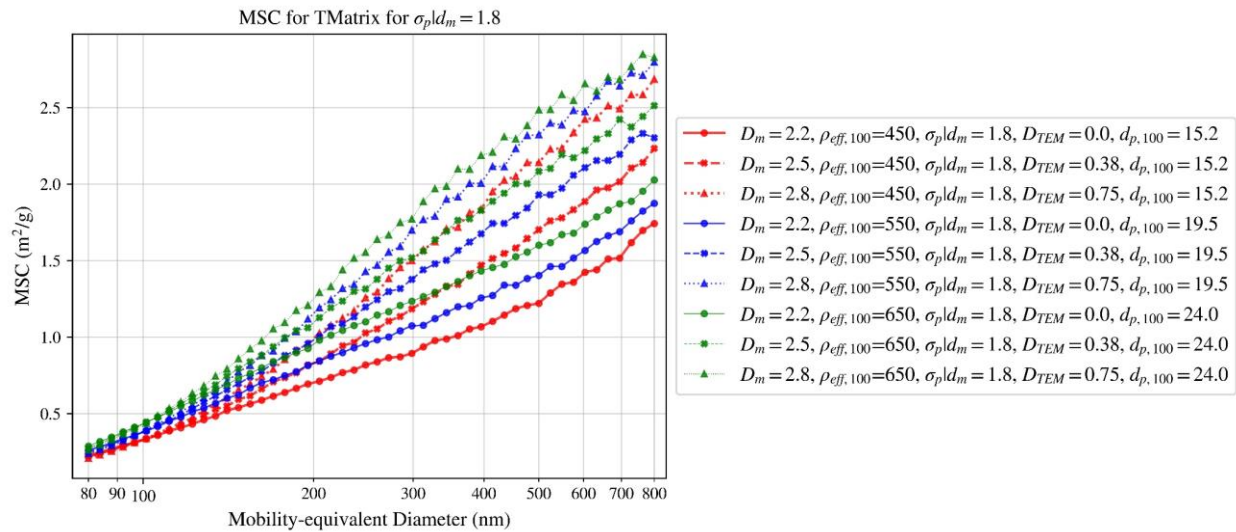


Figure 93

18. Conclusion

???

References

- [1] Jacobson, M.Z., *Strong radiative heating due to the mixing state of black carbon in atmospheric aerosols*. Nature, 2001. **409**: p. 695.
- [2] Medalia, A.I. and F.A. Heckman, *Morphology of Aggregates—II. Size and Shape Factors of Carbon Black Aggregates from Electron Microscopy*. Carbon, 1969. **7**(5): p. 567.
- [3] Mackowski, D.W. and M.I. Mishchenko, *Calculation of the T matrix and the scattering matrix for ensembles of spheres*. Journal of the Optical Society of America A, 1996. **13**(11): p. 2266-2278.
- [4] Purcell, E.M. and C.R.J.T.A.J. Pennypacker, *Scattering and absorption of light by nonspherical dielectric grains*. 1973. **186**: p. 705-714.
- [5] Bohren, C.F. and D.R. Huffman, *Absorption and Scattering of Light by Small Particles*. null. Vol. null. 1983. null.
- [6] Forestieri, S.D., et al., *Measurement and modeling of the multiwavelength optical properties of uncoated flame-generated soot*. Atmos. Chem. Phys., 2018. **18**(16): p. 12141-12159.
- [7] Olfert, J.S. and S.N. Rogak, *Universal relations between soot effective density and primary particle size for common combustion sources*. Aerosol Science & Technology, 2019.
- [8] Schmidt-Ott, A., *New approaches to in situ characterization of ultrafine agglomerates*. Journal of Aerosol Science, 1988. **19**(5): p. 553-563.
- [9] Forrest, S.R. and T.A. Witten, *Long-range correlations in smoke-particle aggregates*. Journal of Physics A: Mathematical and General, 1979. **12**(5): p. L109-L117.
- [10] Sorensen, C.M., *The Mobility of Fractal Aggregates: A Review*. Aerosol Sci. Technol., 2011. **45**(null): p. 765.
- [11] DeCarlo, P.F., et al., *Particle Morphology and Density Characterization by Combined Mobility and Aerodynamic Diameter Measurements. Part 1: Theory*. Aerosol Science and Technology, 2004. **38**(12): p. 1185-1205.
- [12] Schmidt-Ott, A., et al., *Scaling behaviour of physical parameters describing agglomerates*. Journal of Aerosol Science, 1990. **21**(6): p. 711-717.
- [13] Slowik, J.G., et al., *Particle Morphology and Density Characterization by Combined Mobility and Aerodynamic Diameter Measurements. Part 1: Theory AU - DeCarlo, Peter F.* Aerosol Science and Technology, 2004. **38**(12): p. 1185-1205.
- [14] Medalia, A.I., *Morphology of Aggregates*. J. Colloid Interface Sci., 1967. **24**(3): p. 393.
- [15] Dastanpour, R., et al., *Improved sizing of soot primary particles using mass-mobility measurements*. Aerosol Science and Technology, 2016. **50**(2): p. 101-109.

- [16] Meakin, P., B. Donn, and G.W. Mulholland, *Collisions between Point Masses and Fractal Aggregates*. Langmuir, 1989. **5**(2): p. 510.
- [17] Rogak, S.N., R.C. Flagan, and H.V. Nguyen, *The Mobility and Structure of Aerosol Agglomerates*. Aerosol Sci. Technol., 1993. **18**(1): p. 25.
- [18] Choi, M.Y., et al., *Comparisons of the soot volume fraction using gravimetric and light extinction techniques*. Combustion and Flame, 1995. **102**(1): p. 161-169.
- [19] Dastanpour, R. and S.N. Rogak, *Observations of a Correlation between Primary Particle and Aggregate Size for Soot Particles*. Aerosol Sci. Technol., 2014. **48**(10): p. 1043.
- [20] Seinfeld, J., *Atmospheric Chemistry and Physics of Air Pollution*. null. Vol. null. 1986. null.
- [21] Mulholland, G.W., C.F. Bohren, and K.A. Fuller, *Light Scattering by Agglomerates: Coupled Electric and Magnetic Dipole Method*. Langmuir, 1994. **10**(8): p. 2533-2546.
- [22] Sorensen, C.M., *Light Scattering by Fractal Aggregates: A Review*. Aerosol Sci. Technol., 2001. **35**(2): p. 648.
- [23] Yang, B. and U. O. Koju, *Soot processes in a strongly radiating turbulent flame from laser scattering/extinction experiments*. Vol. 93. 2005. 289-299.
- [24] Liu, F. and D. Snelling, *Evaluation of the Accuracy of the RDG Approximation for the Absorption and Scattering Properties of Fractal Aggregates of Flame-Generated Soot*, in *40th Thermophysics Conference*. 2008, American Institute of Aeronautics and Astronautics.
- [25] Bond, T.C. and R.W. Bergstrom, *Light Absorption by Carbonaceous Particles: An Investigative Review*. Aerosol Sci. Technol., 2006. **40**(1): p. 27.